UC Santa Cruz

UC Santa Cruz Electronic Theses and Dissertations

Title

Long Duration Gamma-Ray Emission From Thunderclouds

Permalink

https://escholarship.org/uc/item/6009v2kg

Author

Kelley, Nicole

Publication Date

2014

Peer reviewed|Thesis/dissertation

eScholarship.org Powered by the California Digital Library
University of California

UNIVERSITY OF CALIFORNIA
SANTA CRUZ

LONG DURATION GAMMA-RAY EMISSION FROM THUNDERCLOUDS

A dissertation submitted in partial satisfaction of the
requirements for the degree of

DOCTOR OF PHILOSOPHY

in

PHYSICS

by

Nicole A. Kelley

December 2014

The Dissertation of Nicole A. Kelley
is approved:

Professor David M. Smith, Chair

Professor Joseph R. Dwyer

Professor Patrick Y. Chuang

Dean Tyrus Miller
Vice Provost and Dean of Graduate Studies

Copyright © by

Nicole A. Kelley

2014

Table of Contents

List of Figures v

List of Tables vii

Abstract viii

Dedication x

Acknowledgments xi

1 Introduction 1
- 1.1 Electric fields inside thunderstorms . . . 2
- 1.2 Relativistic Runaway Electron Avalanches . . . 8
- 1.3 Gamma-ray Glow Observations . . . 13
- 1.4 High Energy Atmospheric Physics . . . 17

I Instrumentation 21

2 ADELE Instrument - Version 1.0 22
- 2.1 Instrumentation . . . 23
- 2.2 ADELE 2009 Campaign . . . 29
- 2.3 ADELE Calibrations . . . 36
  - 2.3.1 Method 1 . . . 36
  - 2.3.2 Method 2 . . . 39
  - 2.3.3 Method Comparison . . . 42

3 ADELE Instrument - Version 2.0 44
- 3.1 New Instrument . . . 45
- 3.2 HS3 Mission . . . 47

3.2.1 Testing 48
3.2.2 Integration 51
3.2.3 Mission 52
3.3 Hurricane Hunters 53

II Gamma Ray Glow Measurements 56

4 The ADELE Glows 57
4.1 Introduction 57
4.2 Interpreting the ADELE Results 59
4.3 Overview of the ADELE Glows 61
4.4 Glows and their relationship to lightning 68
4.4.1 The Glow Lightning Model 76

5 Relativistic electron avalanches as a thunderstorm discharge competing with lightning 88
5.1 Introduction 88
5.2 Results 91
5.3 Conclusion 98
5.4 Methods 99

6 Conclusion 104

List of Figures

1.1 Cloud charge structure 4
1.2 Temperture dependence of charge separation 5
1.3 Convective charging of thunderclouds. 7
1.4 Types of lightning. 9
1.5 Bethe-Bloch curve for an electron in air 11
1.6 RREA versus Relativistic Feedback 14
1.7 McCarthy and Park glows 15

2.1 1st ADELE Instrument CAD 26
2.2 ADELE Signal Flow 27
2.3 ADELE Instrument Photos 28
2.4 Gulfstream V 30
2.5 ADELE's TGF 31
2.6 ADELE Sensitivity 33
2.7 Lightning within 10 km of ADELE 35
2.8 ADELE Source Calibrations - before improvements 41
2.9 ADELE Source Calibrations - after improvements 43

3.1 Lateral Vibration Testing Results 49
3.2 Inline Vibration Testing Results 50
3.3 Hurricane Hunters Plane 54

4.1 McCarthy and Parks Glow compared to an ADELE Glow 60
4.2 Hardness and Top/Bottom Response for the ADELE Insturment . 62
4.3 Time profiles of the ADELE Glows 1 64
4.4 Time profiles of the ADELE Glows 2 65
4.5 Hardness versus top/bottom for the ADELE glows 69
4.6 Hardness in the top vs bottom detector during glows 70
4.7 Glow Nearby Lightning Activity 1 72

4.8 Expected Counts Model over Glows 79
4.9 Expected Model Peaks versus Real Glow Count Peaks 80
4.10 Glow Distance versus Hardness 82
4.11 Glow Distance versus Top/Bottom 83
4.12 Glow Distance versus Glow Duration 85
4.13 Glow Distance versus Glow Intensity 86
4.14 Lightning Activity Around Glows and Expected Glows 87

5.1 Time profile of the August 21 glow compared to others 93
5.2 Meteoroligcal scan during bright glow with cloud structure 95
5.3 Top/Bottom and Spectral Difference between Aug. 21 Glows and Models 102

List of Tables

2.1 Pulser settings for large plastic calibrations 38

4.1 Table of ADELE Glows 67

Abstract

Long Duration Gamma-ray Emission from Thunderclouds

by

Nicole A. Kelley

Gamma-ray glows are long duration emission coming from thunderclouds. They are one example of high-energy atmospheric physics, a relatively new field studying high-energy phenomena from thunderstorms and lightning. Glows arise from sustained relativistic runaway electron avalanches (RREA). Gamma-ray instruments on the ground, balloons and airplanes have detected glows. The Airborne Detector for Energetic Lightning Emissions (ADELE) is an array of gamma-ray detectors, built at the University of California, Santa Cruz. ADELE detected 12 gamma-ray glows during its summer 2009 campaign.

ADELE was designed to study another type of high-energy atmospheric physics, terrestrial gamma-ray flashes (TGFs). TGFs are incredibly bright, sub-millisecond bursts of gamma-rays coming from thunderstorms. ADELE was installed on NCARs Gulfstream V for the summer of 2009. While many glows were detected, only one TGF was observed. In this thesis I present a detailed explanation of the 2009 version of ADELE along with the results of the 2009 campaign.

ADELE was modified to become a smaller, autonomous instrument to fly on the NASA drone, a Global Hawk. This was a piggyback to NASAs Hurricane

and Severe Storm Sentinel mission. These flights took place during the summer of 2013. The following summer, ADELE flew on an Orion P3 as a piggyback of NOAAs Hurricane Hunters. This newer, modified instrument is discussed in detail in this thesis.

The 12 gamma-ray glows from the 2009 campaign are presented, with information about nearby lightning activity. I show that lightning activity is suppressed after a glow. This could be from the glow causing the cloud to discharge and therefore reduce the lightning activity. It is also possible that glows can only occur once lightning activity has diminished. Lightning is also used to find a distance to the glow. Using this distance, it is found that the brightness of glow cannot be explained as a function of distance while the duration of the glow is related to the distance.

The glow measured on August 21, 2009 was 20 times brighter than any other glow. This glow was modeled most extensively and it was found that ADELE was in the end of a downward facing avalanche, implying that is was flying between the upper positive and negative screening layer of the thunderstorm. The brightness of this glow also showed that the avalanche was approaching the levels necessary for relativistic feedback. I also show that this glow provides a significant discharge current and for a short while is discharging the cloud as much as nearby lightning.

To my parents,

Rod and Cristina Kelley,

whose love and never ending support is the reason this thesis exists.

Acknowledgments

I would like to thank my advisor, David Smith, for his patience, support and guidance. I could not have imagined having a better mentor and advisor and I will always be a better scientist because of him. Thank you to my other committee members: Joseph Dwyer and Patrick Chuang. Their comments and insights were very much appreciated. Thank you to my coworker, Greg Bowers. It has been a joy to work with him these past few years, even with our little disagreements. We have accomplished some great things and had fun doing it too.

Thank you to my amazing group of Santa Cruz friends. There were many that helped keep me sane these past few years but special thanks to Carena, TJ, Eddie, Omar, Rachel, Laura, Colleen and Tim. Santa Cruz will always have a special place in my heart.

Thank you to my wonderful family. Mom, Dad, Billy, Faith and Elana: thank you for always beliveing in me and always being there for me no matter what. To Nannie Annie, Grandma, Grandpa, Auntie, Jeff, Auntie Kris, Uncle Jim, Uncle Frank, Zach and Adam: I could not have asked for a better family. Thank you for all your support.

And finally, thank you to the best husband, Chris. You are my sanity, my motivation and my guide.

Chapter 1

Introduction

In 1925, C.T.R. Wilson hypothesized that the electric fields in thunderclouds could accelerate electrons to speeds high enough to emit x-ray and gamma rays via bremsstrahlung (Wilson, 1925). There were serveral experiments from 1930 onward (Schonland, 1930; Halliday, 1934; Clay, Jongen & Aarts, 1952; Whitmire, 1979), however, it was not until the 1980s that clear evidence of this emission existed (Parks et al., 1981). Since then, the field of high-energy atmospheric physics (HEAP) (Dwyer, Smith & Cummer, 2012) has taken off. With measurements occurring in Europe, Asia, North and South America, the field has intrigued people worldwide. HEAP includes the measurement of bright bursts of gamma radiation seen from space called terrestrial gamma-ray flashes (TGFs), short bursts of x-rays from lightning stepped leaders, and long duration gamma ray glows.

While the models behind each of these phenomena are different, these events all arise from electrons being accelerated by electric fields related to thunderstorms or lightning and then emitting energetic photons via bremsstrahlung. In this thesis, I will briefly discuss all three high-energy emissions from thunderstorms, but will mainly focus on the long duration emission, gamma-ray glows. These events are very common and may play an important role in the overall charging/discharging of a thundercloud.

The Airborne Detector for Energetic Lightning Emissions (ADELE) is an array of gamma-ray detectors built at the University of California, Santa Cruz. It has been deployed on several missions around North America in both airplanes and on the ground. ADELE has detected TGFs, x-ray stepped leaders and gamma-ray glows. Again, while all measurements will be briefly explained, the many measurements of gamma-ray glows by ADELE will be discussed in great detail.

1.1 Electric fields inside thunderstorms

Thunderstorms are defined as clouds containing thunder (MacGorman & Rust, 1998). Thunder is the sonic shock wave from the rapid expanison of air caused by lightning. Lightning is the cloud's response to equalize the large build up of charge that occurs within it. There are multiple theories that can explain how clouds charge. All models involve hydrometeors. Hydrometeors are different

types of water particles in clouds. Liquid water particles are called cloud water droplets, or droplets. Solid particles can be either snow (lowest density), graupel (intermediate densities), or hail (greatest density) (MacGorman & Rust, 1998).

Charging mechanisms are divided into precipitation and convective mechanisms (MacGorman & Rust, 1998). All methods need to account for the measured charge structures of thunderstorms. Most thunderstorms are thought to have a main upper postive and lower negative, or dipole structure. Many thunderstorms have a lower positive charge center, and the cloud is called a tripole. Figure 1.1 shows a simplistic cartoon of the charge structure in thunderclouds. In addition, clouds can also have an upper positive screening layer (Vonnegut et al., 1962; Marshall et al., 1989).

Precipitation mechanisms involve precipation as the primary means to separate charge around the cloud. At low temperatures, below -15° C, heavier hydrometeors, such as hail, rain or graupel, are more likely to carry negative charge while lighter particles, such as snow or smaller water droplets, are more likely to carry positive charge. This has been showed experimentally. The large droplets fall to the bottom regions of the cloud, creating the main negative charge center of the cloud(Williams, 1987). Above -15° C, the larger, heavier particles are more likely to be positively charged. This explains the lower positive charge region of the tripole charge structure. Figure 1.2 shows the precipitation mechanism.

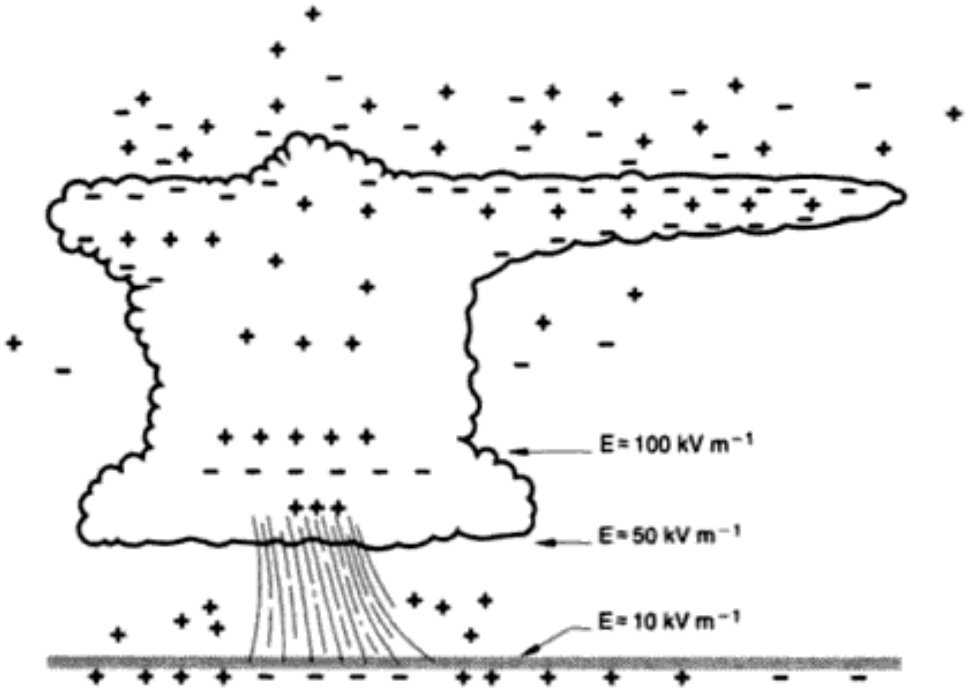


Figure 1.1: Figure from (MacGorman & Rust, 1998). The tripole charge structure of a thunderstorm with upper positive screening layer included.



Figure 1.2: Figure from (Saunders, 2008). The temperature dependence of the seperation of charge on water particles in precipitation mechanisms.

Convection mechanisms rely on a net positive charge that is present during fair weather conditions. Positive ions near the ground are brought into the cloud and carried upward via convection(Figure 1.3a). A negative screening layer forms and then is moved down the sides of the cloud through convective motions (Figure 1.3b). Negative charges are moved into the vast majority of the bottom of the cloud while positive charges continue to be brought into the cloud (Figure 1.3c). This mechanism can explain the tripole moment observed in thunderstorms.

The separation of charge inside clouds creates electric fields that can accelerate particles and initiate lightning. Lightning occurs when the electric field approaches 150 kV/m and rarely in fields higher than that (Marshall & McCarthy, 1995). Lightning is a means to neutralize the electric field, by moving large amounts of charge in a short amount of time. A typical lightning flash moves about 20 Coulombs of charge in about a second (Uman, 2001).

Lightning can move charge between clouds (intercloud), within a cloud (intracloud) and between clouds and the ground (cloud-to-ground). Both intercloud and intracloud are referred to as IC lightning while cloud-to-ground lightning is called CG. The polarity of the lightning is indicated before the abbreviation, such as +IC when positive charge is moved downward and when negative charged is moved upward versus -IC when negative charge is moved downward and positive charge upward. The different types of lightning are shown in Figure 1.4. There

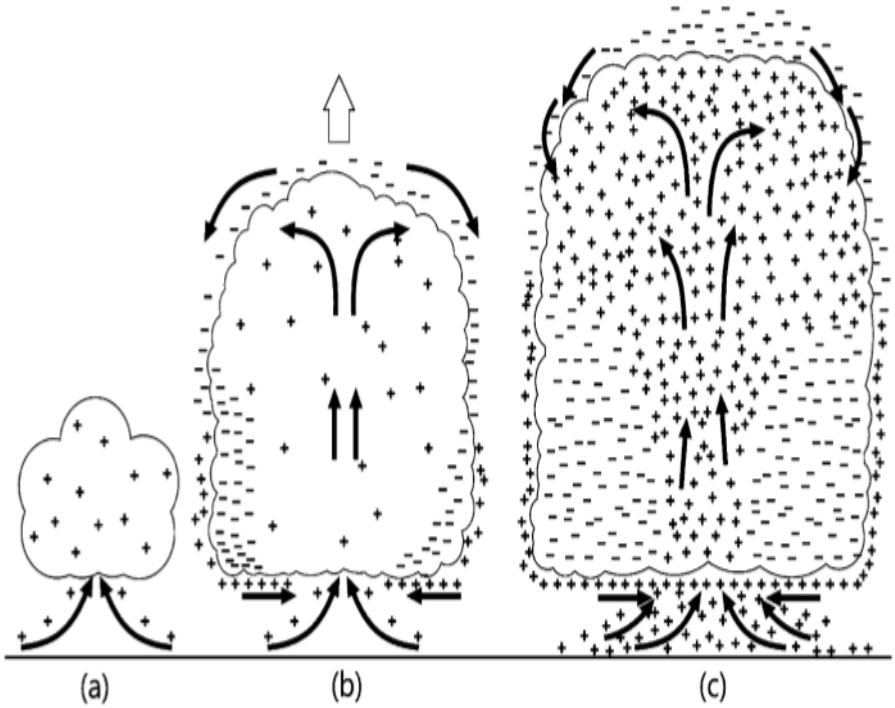


Figure 1.3: Figure from (Saunders, 2008). The convective charging mechanism of thunderclouds.

are four types of CG lightning: upward negative, downward negative, upward positive, downward positive (**?**).

In addition to lightning, thunderstorms have other phenomena that are the result of large electric fields inside the cloud. Section 1.4 will discuss the high-energy events resulting from electric fields within thunderstorms. In addtion, thunderstorms can create sprites, elves, blue jets, and giant jets. Sprites are streamer discharges that occur around 80 km altitude. They occur when a large +CG flash changes the electric field configuration in the cloud below (Dwyer & Uman, 2014). Elves are rings of light about 300 km across in the lower ionosphere. They are caused by the electromagnetic pulse generated by the lightning return stroke below (Dwyer & Uman, 2014). Blue jets and gigantic jets are analogous to upward lightning. They are able to reach altitudes of up to 40 km, for blue jets, and 90 km for gigantic jets (Dwyer & Uman, 2014).

1.2 Relativistic Runaway Electron Avalanches

Electric fields will cause electrons to accelerate. Electrons in electric fields in air can run away to relativistic energies with the right set of initial conditions. The Bethe-Bloch curve shown in Figure 1.5 shows how the force of friction can decrease with increasing energy. This is because for a certain regime of energies, the faster a particle travels, the less time it will spend interacting with other particles,

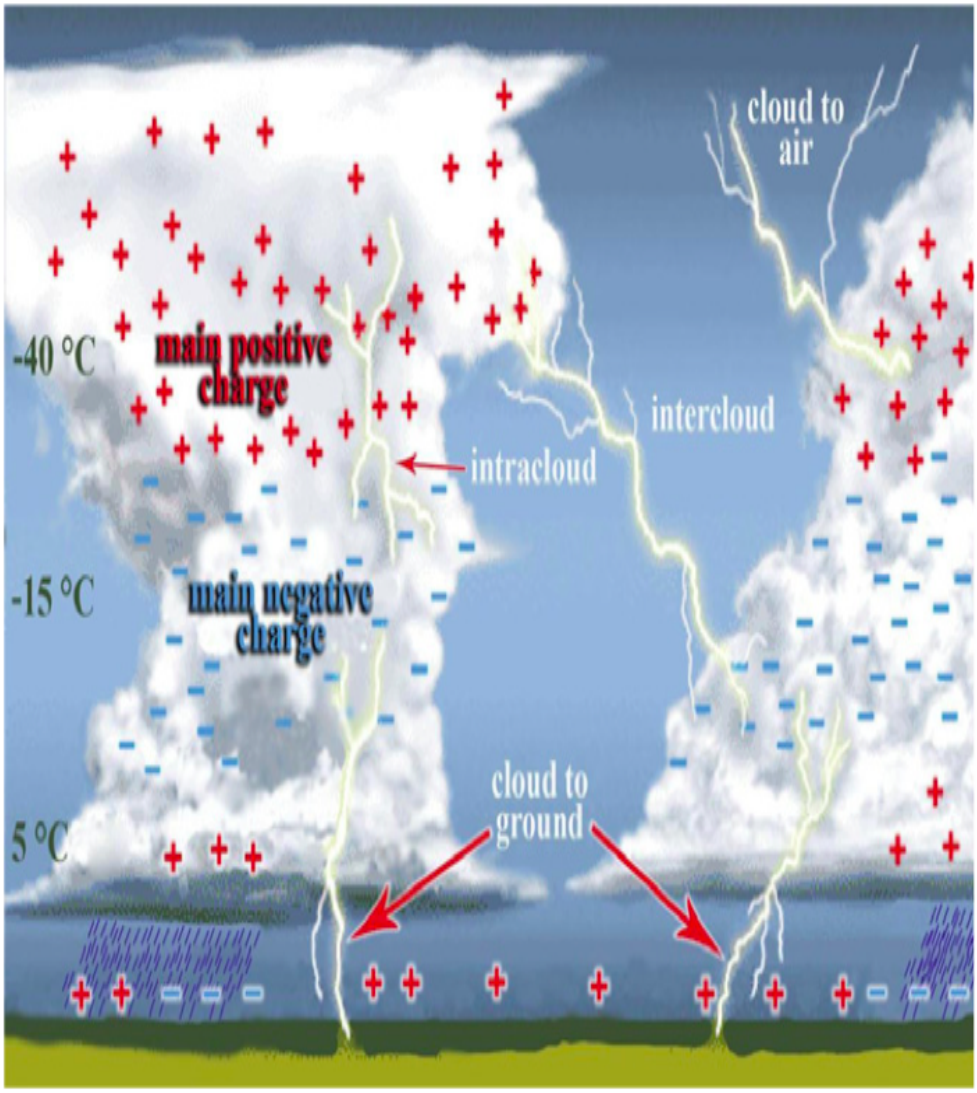


Figure 1.4: Figure from (Dwyer & Uman, 2014). Different types of lightning based on the charge in thunderclouds.

thereby experiencing less friction. For any electric field above the breakeven field, E_b, an electron with enough energy, ($\epsilon > \epsilon_{th}$) can run away. This is because the force from the electric field is greater than the force the electron experiences from friction. For electric fields equal to or greater than E_c, all electrons, thermal and relativistic can run away. This is known as "cold runaway" Gurevich (1961); Dwyer (2004). For typical electric fields found in thunderstorms, electrons must already be relativistic in order to run away. These relativistic seed particles can come from cosmic rays, radioactive decays, or thermal electrons that have been accelerated to relativistic energies in high-electric field regions, such as those in lightning stepped leaders.

Gurevich, Milikh & Roussel-Dupre (1992) proposed the relativistic runaway electron avalanche (RREA) model to explain long-duration gamma-ray glows that were previously measured. In this mechanism, Møller scattering is included. A relativistic electron scatters with a non-relativistic electron, sharing its energy, so that both electrons become relativistic. This introduces avalanche multiplication so that one relativistic seed electron will result in an exponential growth of relativistic electrons. All these electrons emit gamma rays via bremsstrahlung after passing by positive air nuclei. Bremsstrahlung is "braking radiation", that results when a charged particle is slowed down by another charged particle and a gamma ray is emitted to conserve energy.

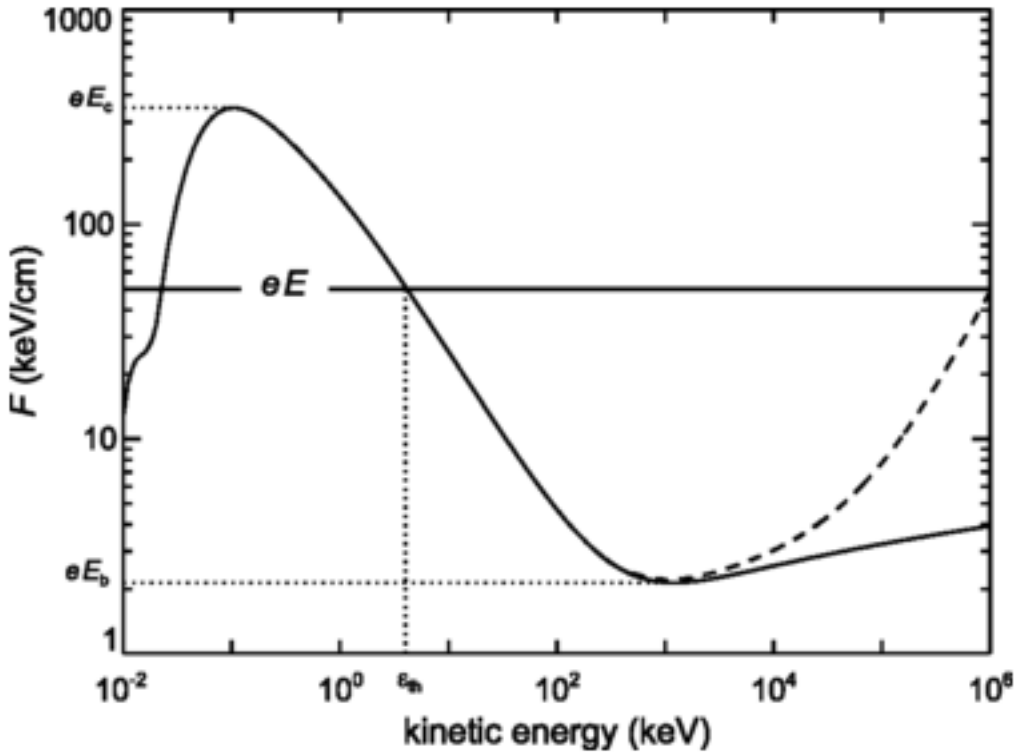


Figure 1.5: Figure from (Dwyer, Smith & Cummer, 2012). The frictional force on an electron moving through air at STP as a function of the electron kinetic energy. The line labeled eE is the force the electron experiences in a 5.0×10^6 V/m electric field.

RREA has been shown to provide the correct energy spectra for both TGFs and gamma-ray glows (Tsuchiya et al., 2007; Dwyer & Smith, 2005). However, RREA alone cannot account for the brightness observed in TGFs. Relativistic feedback includes positron and gamma-ray feedback and can account for the intensities of TGFs (Dwyer, 2008). Positrons are created via pair production. Pair production occurs when a high-energy photon interacts with a nucleus and creates a positron and electron. The electrons continue along in the electric field, sometimes emitting a gamma ray or many gamma rays via bremsstrahlung. The positron will turn around in the electric field and travel in the opposite direction for a considerable distance, since the cross-section for positron annihilation decreases with energy. If these positrons travel to the beginning of the avalanche region and Bhabha scatter with an atomic electron, they will produce a relativistic electron that can start a new avalanche. For gamma-ray feedback, gamma rays can Compton backscatter off an electron and travel back to the beginning of the avalanche region. At the beginning of the avalanche, the gamma rays can either be photoelectrically absorbed by an atom, emitting a new electron to start a new avalanche or Compton scatter, accelerating electrons to relativistic energies, starting a new avalanche (Dwyer, 2007). Relativistic feedback results in an exponential growth of avalanches and can account for the extreme intensities observed with TGFs. Figure 1.6 shows the difference between runaway of a single electron,

RREA and relativistic feedback and how when more physics is included in the model, the resulting high-energy population of electrons grows.

1.3 Gamma-ray Glow Observations

Gamma-ray glows are long duration gamma ray emission coming from thunderstorms. They last from a couple of seconds to several tens of minutes (Eack et al., 1996b; Tsuchiya et al., 2011; Torii, Takeishi & Hosono, 2002; Chilingarian et al., 2010) and are due to sustained RREA (Tsuchiya et al., 2007; Babich et al., 2010). In the 1980's McCarthy and Parks were the first to conclusively detect high-energy emission from thunderstorms. They flew a NaI scintillator on a NASA F-106 jet and were sensitive to energies in the range of 5-110 keV (McCarthy & Parks, 1985; Parks et al., 1981). Figure 1.7 shows three of their observed glows during a flight. It is interesting to note that the first two glows' abrupt endings are coincident with lightning. This is most likely due to lightning rapidly discharging the electric field, so sustained RREA is no longer possible.

Gamma-rays glows have been measured from balloons, airplanes and from the ground. Eack et al. found several instances of glows from balloon borne experiments. They found that the glows were coincident with high electric fields in the cloud (Eack et al., 1996b,a, 2000). Besides the McCarthy and Parks measurements from an airplane, the ADELE instrument measured 12 gamma-ray

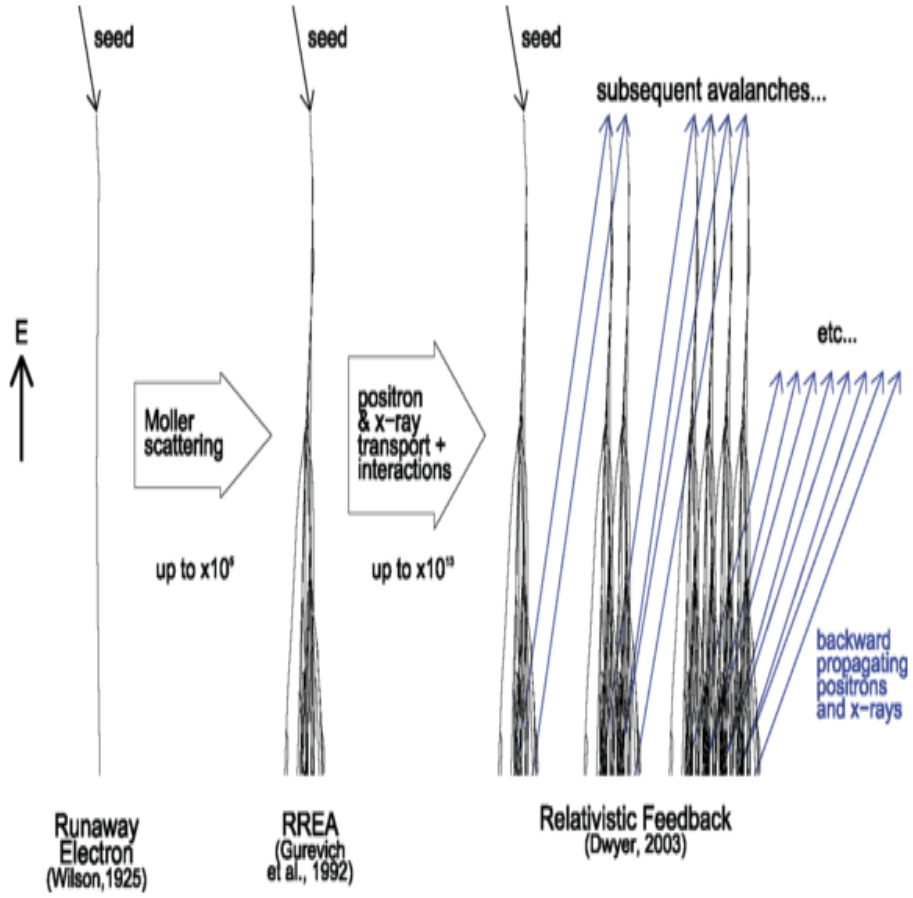


Figure 1.6: Figure from (Dwyer, Smith & Cummer, 2012). Comparison between a single runaway electron, RREA and relativistic feedback showing the different physics that is added to each model and the resulting electron population growth.

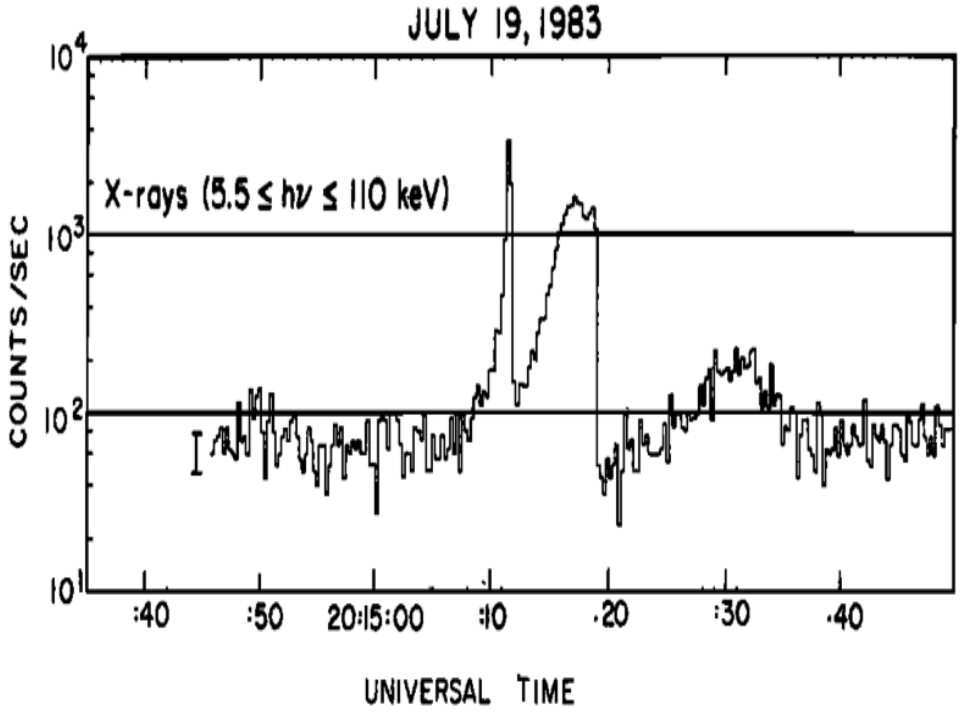


Figure 1.7: Figure from (McCarthy & Parks, 1985). Three glows during the 1983 McCarthy and Parks flights through thunderstorms. They are at :10, :15 and :30. The first two glows are coincident with lightning terminating them.

glows during its 2009 flight on a NOAA Gulfstream V. These will be discussed in Chapters 4 and refchapbrightglow. Ground measurements need to happen on either high mountains or in places where the storms come very low, as do winter thunderstorms in Japan (Torii, Takeishi & Hosono, 2002), since the atmosphere attenuates the gamma rays very quickly. The first two groups to measure glows from the ground were Brunetti et al., who found a spectral component up to 10 MeV (Brunetti et al., 2000), and Chubenko et al., whose spectrum was consistent with bremsstrahlung from runaway electrons (Chubenko et al., 2000). Both these measurements took place at high altitudes. From thunderstorms in Japan, both at high elevation and at sea level during winter, Tsuchiya et al. (2007, 2011) showed that glows have spectra consistent with RREA. Torii et al. (2011) showed the movement of a glowing cloud in a winter Japanese thunderstorm.

Gamma-ray glows are called different things by other groups. Chilingarian et al. refers to them as thunderstorm ground enhancements (TGEs) (Chilingarian, Vanyan & Mailyan, 2013). They have an array of detectors at Aragats, 3200 meters above sea level. They have detected hundreds of enhancements of high-energy electrons, gamma rays and neutrons (Chilingarian et al., 2010; Chilingarian, Mailyan & Vanyan, 2012). They have also brought attention to a possible sub-group of glows called modification of the energy spectra (MOS). This is a slight modification/amplification of a cosmic ray shower (Chilingarian, Hovsepyan & Kozliner,

2013). It is possible that MOS occurs when the electric field is low enough that there is very little avalanche multiplication and hence very littlefeedback, so all growth of the population is from the seed population. Gurevich et. al refer to glows as growth of the gamma-ray background (GRB) (Gurevich et al., 2011a). Their measurements occur at Tien-Shan Mountain Cosmic Ray station, 3400-4000 meters above sea level. In addition to glows, events lasting 100's of milliseconds were also observed (Gurevich et al., 2011b). These are a new class of events that have not been seen by any other group.

1.4 High Energy Atmospheric Physics

High energy atmospheric physics (HEAP) is a relatively new field consisting of high-energy measurements from thunderclouds and lightning(Dwyer, Smith & Cummer, 2012). So far this involves the theories and observations behind gamma-ray glows, terrestrial gamma-ray flashes (TGFs), and x-rays from lightning stepped leaders.

Gamma-ray glows are instances where RREA is sustained for relatively long periods of time. In Chapter 5, we show a gamma-ray glow that approaches the level necessary for feedback. In the steady state, relativistic feedback enhances

the flux of runaway electrons by a multiplicative factor:

$$F_{RREA} = F_0 \frac{\exp(\xi)}{1-\gamma} \tag{1.1}$$

where γ is the feedback factor, ξ is the number of e-folding lengths and F_0 is the background flux of relativistic seed electrons. For $\gamma << 1$, the system is in a state where the flux of seeds is larger than electrons generated through feedback (Dwyer, Smith & Cummer, 2012). As γ approaches 1, feedback begins to dominate, and feedback begins to discharge the cloud and at a similar rate to that of its charging, explaining long-duration emission of gamma rays (glows). When $\gamma \geq 1$, feedback dominates and the system becomes unstable and equation 1.1 no longer applies. This scenario would explain a terrestrial gamma-ray flash (TGF).

TGFs are bright bursts of emission, lasting between tens of microseconds and a millisecond. They were first discovered by the Burst and Transient Source Experiment (BATSE) onboard the Compton Gamma-ray Observatory (CGRO) (Fishman et al., 1994). Since then, three other satellites have made numerous observations of TGFs: the Reuvan Ramaty High Energy Solar Spectroscopic Imager (RHESSI) (Smith et al., 2005), AstroRivelatore Gamma a Immagini Leggero (AGILE) (Marisaldi & Cattaneo, 2010) and both the Gamma ray Burst Monitor (GBM) and the Large Area Telespcope (LAT) onboard Fermi (Briggs et al., 2010). TGFs have spectra similar to glows but are orders of magnitude brighter (Tsuchiya et al., 2007; Chilingarian et al., 2010).

X-ray emission from stepped leaders is common with -CG lightning. X-rays from lightning were first measured in 2001 (Moore et al., 2001). Since then studies of both natural and triggered lightning have led to the conclusion that x-ray stepped leaders have a different spectrum than RREA (Dwyer, 2004). Cold runaway can explain the spectrum of stepped leaders. Cold runaway is possible because of the high electric fields at the end of the stepped leaders. The high electric field accelerates nearly all thermal electrons to relativistic energies but this occurs over a very small region before signigficant avalanche multiplication and a very large population can be created. These relativistic electrons may also explain the seed population necessary for TGFs (Celestin & Pasko, 2011).

Electric fields in thunderstorms can modify and amplify electrons from other processes. TGFs may just be the amplification of the electrons from lightning stepped leaders. Dwyer shows that the luminosity of electrons per second from a stepped leader is 10^{16}, which could be a large enough seed population to be amplified by RREA to become a TGF (Dwyer et al., 2010). Chilingarian showed the modification of cosmic-rays by the electric fields in thunderstorms can account for a large number of glows measured from the ground (Chilingarian, Hovsepyan & Kozliner, 2013). In both these cases, the electric field of the thunderstorm modifies an energetic seed population.

It is possible that glows play important role in the overall charging of the

cloud. In Chapter 5, I show that glows can discharge a cloud as much as lightning can. There is also a competition between lightning and glows. Tsuchiya found the glows become spectrally harder as time goes on and are terminated by lightning, showing how lightning shuts the electric field off suddenly (Tsuchiya et al., 2013). Chilingarian and Mkrtchyan show that the lower positive charge region needs to exist in order to be able to measure a glow from the ground. This brings the electric field to a low enough altitude so they are able to measure the gamma rays from the RREA (Chilingarian & Mkrtchyan, 2012).

Part I

Instrumentation

Chapter 2

ADELE Instrument - Version 1.0

The Airborne Detector for Energetic Lightning Emissions was built at the University of California, Santa Cruz by Professor David Smith, then graduate students Bryna Hazelton and Brian Grefenstette, then undergraduate Alex Lowell, engineer Forest Martinez-McKinney, and FPGA programmer Zi Yan Zhang. The purpose of ADELE is to measure to TGFs at the TGF production altitude, namely inside thunderstorms. The design was optimized for detecting TGFs as they were understood in the mid-2000s. It was designed and built over two years between 2007 and 2009 and first deployed in 2009 on a NOAA Gulfstream V. The Gulfstream V chased thunderstorms in the Colorado and Florida regions of the United States. The second campaign was a ground campaign that involved ground storm chasing in both New Mexico and Florida, taking advantage of ADELE's

mobility but not its capability to be airborne.

2.1 Instrumentation

ADELE 2009 was an array of 6 gamma-ray detectors. The configuration consisted of two sensor heads, each with three scintillators. Each sensor head had a 5" diameter × 5" long sodium iodide (NaI) scintillator, a large 5" × 5" plastic scintillator and a small 1" × 1" plastic detector. All the scintillators are paired to photomultiplier tubes (PMT) where the signal is amplified depending on the gain voltage applied. In each sensor head, there is also a blank PMT that is used to rule out electromagnetic noise. The different detector types complement each other. Plastic detectors have a very fast response to incoming photons, a few nanoseconds, while the response of NaI crystals is about 10 times slower. These response times become longer when the signal is amplified by a PMT. Faster response times of a detector allow for higher throughput and count rates. Since TGFs are incredibly bright, about 10^{17} photons at the source, it was very important that ADELE could count up to millions of counts per second.

The time resolution of plastic scintillators allows for detection of high fluence events. The NaI crystals are used to account for the poor energy resolution of plastic. NaI has much higher light output so it is much better for spectroscopic resolution but because of its high light output, its efficiency at stopping incoming

particles, and its long pulses. NaI detectors are more likely to saturate at high count rates. The small plastic detector is to help ensure that at least one detector will not saturate during a TGF. Since the small plastic detector is much smaller, the cross-section for stopping gamma rays is much smaller. Only very bright events that are very close would challenge the limits of the small plastic detector.

The signals out of the plastic and empty PMTs are negative polarity pulses that are clamped, amplified, digitized and split into four energy channels through use of a comparator. The four energy channels correspond to approximate cutoffs of 50 keV, 300 keV, 1 MeV and 5 MeV. The square, digitized signals are sent to a field programmable gate array (FPGA) where the upward transitions between 0 and 1 are counted and the amount of time the signal spends high is counted. The FPGA sampled the output of the plastic PMTs at 200 MHz. The transitions correspond to incoming counts in a given energy channel while the amount of time spent high corresponds to a deadtime, time the instrument is unresponsive to new counts. These counts and deadtimes are binned into 50 μs rates and sent to a computer. The computer records all 50 μs plastic data to hard drives but also performs a quick search algorithm looking for excesses in the data on a 1 ms timescale. These excesses are used as a trigger to initiate another mode of data acquisition.

The NaI signal is split into two. One of those NaI signals is sent to a Gage

flash card. This card records the full waveform of the NaI PMT for 1 second when it receives a trigger from the computer monitoring the plastic data or from an external trigger initiated by a person. The card records data from time before and after the trigger. The trigger uses a Gage flash card record the change in the electric field, $d\boldsymbol{E}/dt$, from a flat plate antenna that is external to the airplane or van. $d\boldsymbol{E}/dt$ is a good indication of rapid discharges near the plane, such as would happen when if lightning occurred nearby. The second signal from the NaI is also sent to a Gage peak detect card, where the peak energy is recorded from every incoming photon.

High-voltage power supplies that were controlled by a sensor services board supplied the voltages on all the PMTs. Two Measurement Computing USB boxes with analog to digital and digital to analog converters were used to set the voltage on the sensor services board. The sensor services board also had voltage monitors and temperature monitors. These were returned to the computer though the use of the USB boxes and of a multiplexer on the sensor services board. This data was recorded every second and stored on a computer.

Figures 2.1-2.3 show CAD drawings of the instrument, a flow chart of the ADELE instrument, and pictures of the finished instrument.

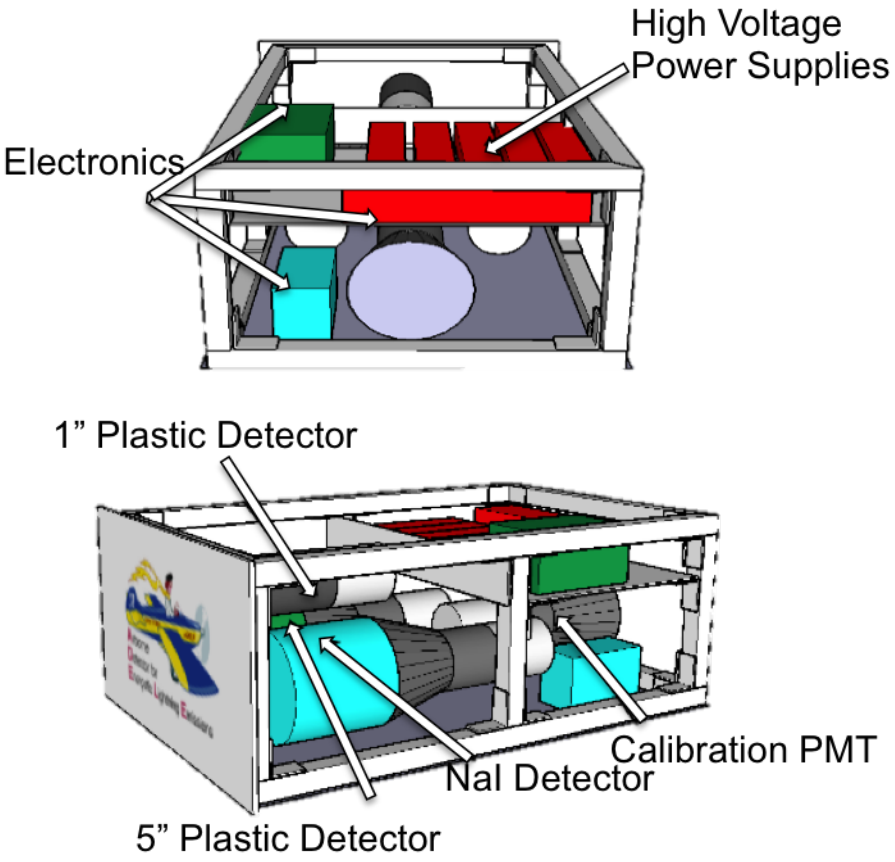


Figure 2.1: CAD drawings of the first ADELE instrument.

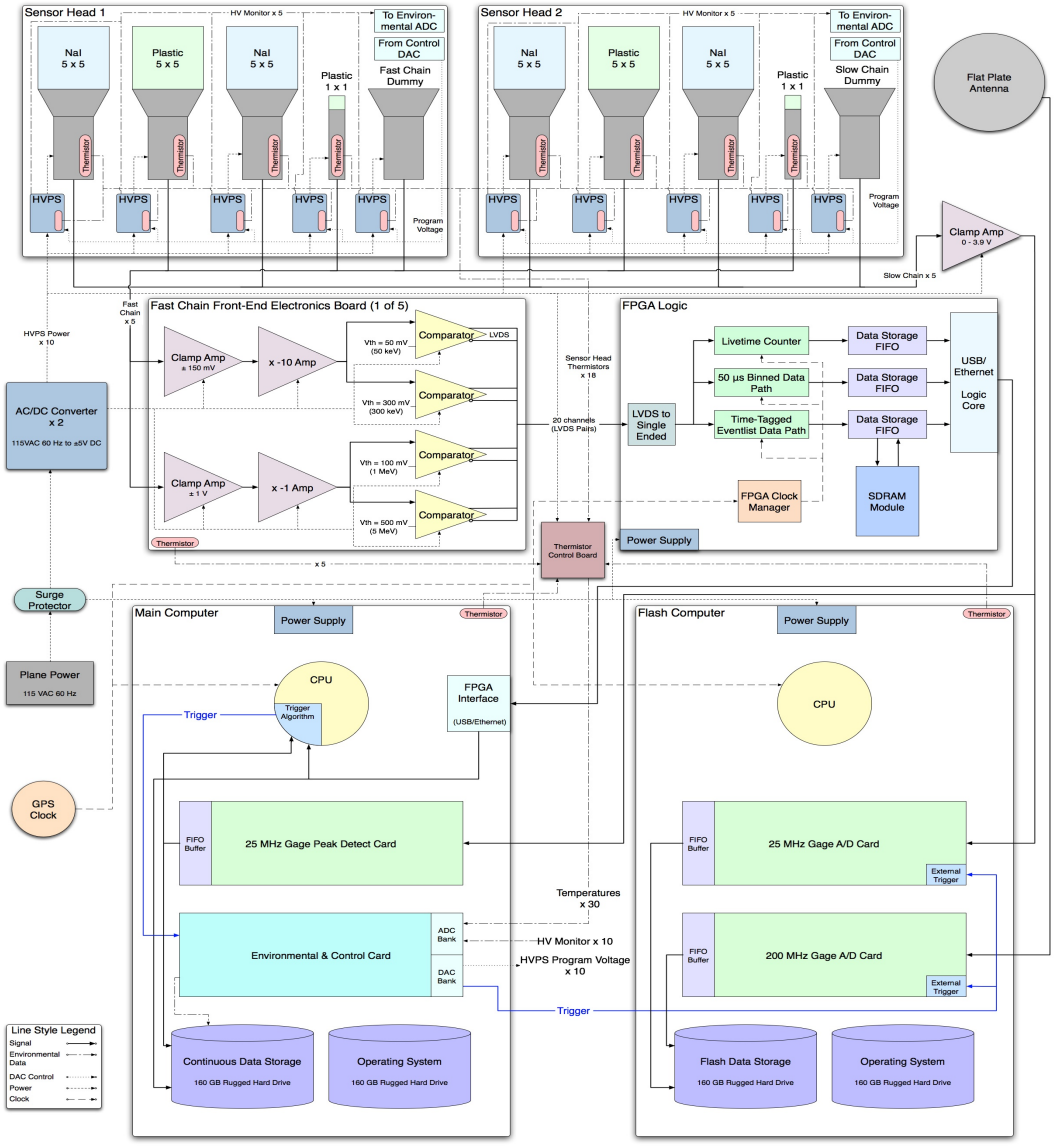


Figure 2.2: A detailed layout of the ADELE instrument



Figure 2.3: Photos of the finished ADELE instrument from the front (left) and back (right).

2.2 ADELE 2009 Campaign

ADELE flew on a Gulfstream V operated by the National Center for Atmospheric Research (NCAR) in the Summer of 2009. The plane had one flight out of Broomfield, Colorado and 8 flights out of Melbourne, Florida. Figure 2.4 is a picture of the plane on the tarmac during operations. ADELE flew for a total of 37 hours. During the flights, there were always at least two scientists operating ADELE, from either UCSC or the Florida Institute of Technology (FIT). During the flights, ADELE measured 12 gamma-ray glows and one TGF. The 12 gamma-ray glows will be discussed in more detail. The discussion in this section has already been published in Smith et al. (2011a) and Smith et al. (2011b).

The ADELE TGF was measured on August 21, 2009 at 20:14:43.437 UTC at a latitude of 31.0746 ° and longitude of 81.5453°, over the southeast coast of Georgia. Figure 2.5 shows the counts in the differential energy channels, 50-300 keV, 300-1000 keV, 1-5 MeV and >5 MeV, of the two large plastic detectors. The counts from differential energy channels are found by subtracting the counts from the next highest energy channel.

Both the National Lightning Detection Network (NLDN) and Weatherbug Total Lightning Network (WTLN) measured a +IC cloud flash 11 ms second before ADELE measured the TGF. These networks detected a lightning flash approximately 10 km away from ADELE. From Monte Carlo simulations of relativistic



Figure 2.4: NOAA's Gulfstream V being towed on the tarmac in Melbourne, Florida.

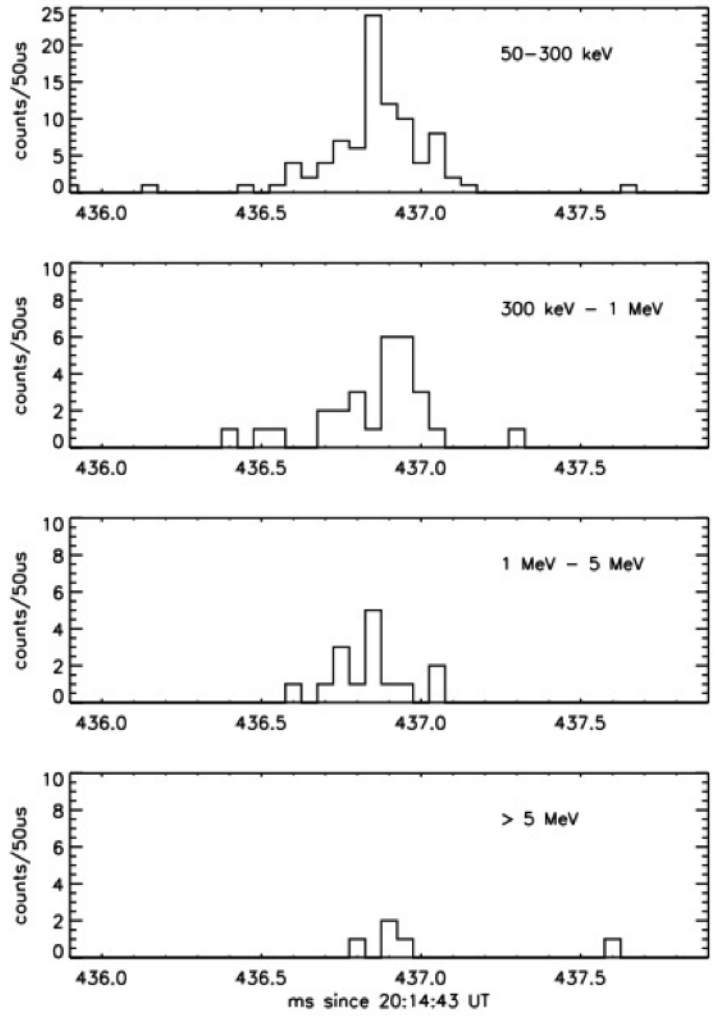


Figure 2.5: The first and only ADELE TGF. Counts/50 μs in the four energy channels of the two large plastic detectors.

feedback, along with simulations of the propogation of gamma rays through the air, airplane and instrument, Figure 2.6 shows the ADELE instrument sensitivity for a typical TGF. This shows the expected counts measured in the ADELE large plastic scintillators from a TGF of 10^{17} gamma rays. The detected TGF was right at the threshold of detection and about 2×10^{17} gamma rays at the source, since ADELE detectred 41 counts.

Another interesting result from the ADELE 2009 campaign is the lack of observed TGFs. ADELE flew close to many lightning flashes that were detected by three lightning networks, NLDN, WTLN and the United States Precision Lightning Network (USPLN). However, only one TGF was observed. Within 10 km, ADELE passed within 1213 unique discharges. Figure 2.6 shows that at 10 km, a TGF would have registered in the plastic detectors with 20 counts, the count threshold used in the search through the 50 μs plastic data, making 10 km the maximum distance ADELE could meausure a typical sized TGF.

Figure 2.7 shows the number of various type of lightning discharges as a function of distance from the plane. Lightning was first matched between the three networks when the time between networks was less than or equal to 1 ms and the distance between the two flashes was less than or equal to 5 km. The bottom right panel of Figure 2.7 shows all discharges with redundancies removed (any match within the time and distance window). If two or three networks saw a lightning

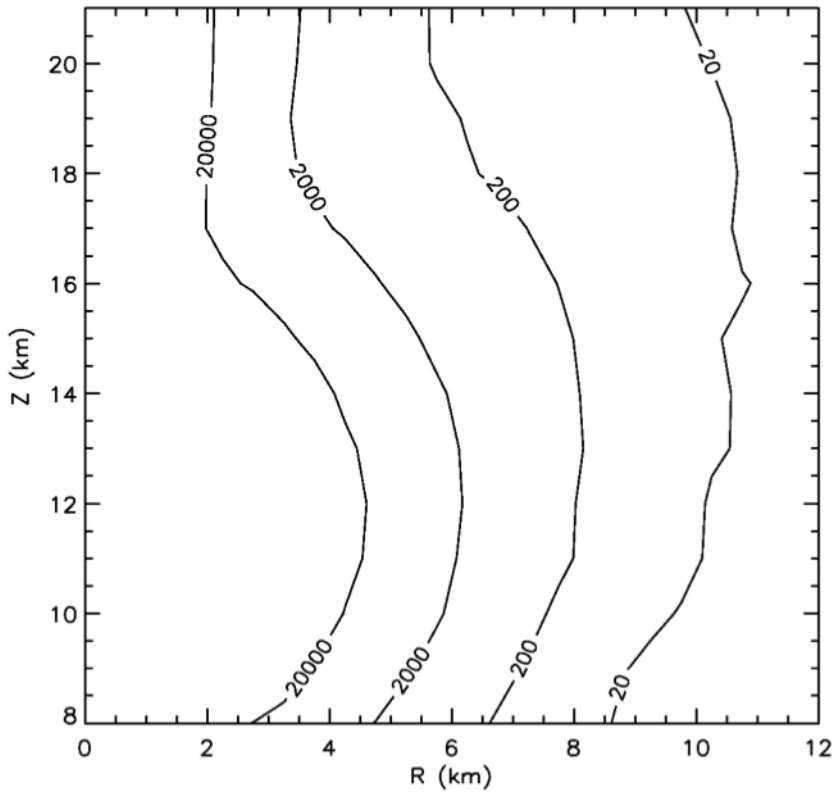


Figure 2.6: The number of expected counts from a TGF with 10^{17} photons in the large plastic detectors as a function of distance.

discharge within that time and distance window, they were verified to be +CG, -CG, +IC or -IC when all of the networks agreed on their classification. If only one network saw a flash within the 1 ms and 5 km window, then that classification was used. Discharges that were classified as CG that were less than 10 kA in peak current were reclassified as IC (Cummins et al., 1998). These lightning flashes are shown in the top two panels and bottom left panel in Figure 2.7. The bottom left panel in Figure 2.7 shows all flashes and their distance from the plane. A flash was found by combining all events from all three networks, regardless of classification, that were within 1 second and 32 km from the airplane. The distance to the plane was found three different ways: the distance of the closest discharge within the flash, the average distance of all discharges within the flash, and the distance of the farthest discharge within the flash.

The non-detection of TGFs for so many lightning events is the first measurement to rule out TGFs as a primary triggering mechanism for lightning. It also rules out a large, much weaker population of TGFs that were unable to be detected from space. While this population of TGFs can still exist, the ADELE 2009 results ruled out that it is a large, common population.

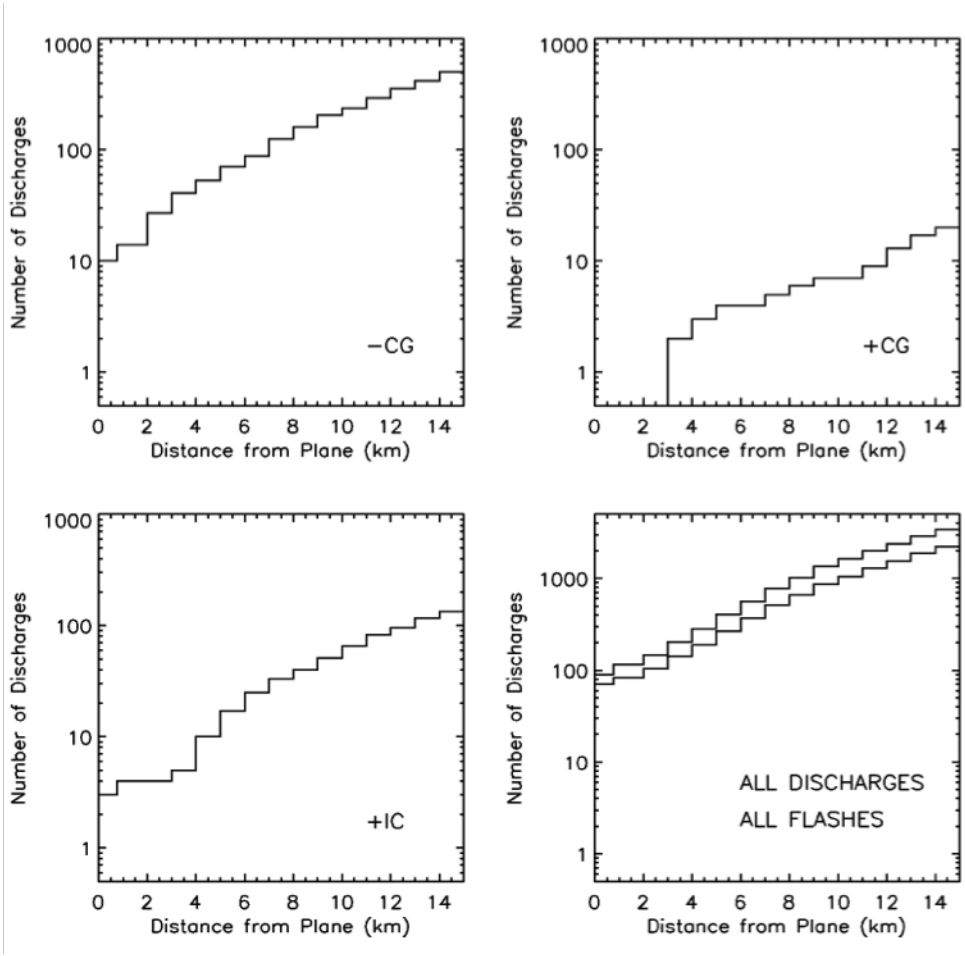


Figure 2.7: The number of cummulative -CG, +CG, +IC and -IC flashes as function of distance from the plane (top two panels and bottom left panel). All lightning flashes, defined as all events within a 1 second and 32 km window, as a function of distance from ADELE (bottom right). All discharges, with redundancies removed (also bottom right).

2.3 ADELE Calibrations

The ADELE PMTs output a voltage pulse that is proportional to the energy deposited in the scintillator. However, this proportionality, the detector gain, depends on the operating voltage of the PMT. In order to know the real energies of incoming photons and other particles, the detectors need to be calibrated. Since the plastic detectors have poor energy resolution and a non-zero percent photopeak, this is not an easy task. The electronic response also needs to be known. Presneted here are two methods used to calibrate the ADELE instrument.

2.3.1 Method 1

The most successful way to calibrate the ADELE plastic detectors is the simplest but does introduce human error. This method involves calibrating the detector and electronics separately. The detector and PMT are calibrated by using the major lines in two gamma ray sealed sources: the 1.408 MeV line of Europium 152 and 662 keV line of Cesium 137. To find the energy response of each line, the source is placed next to each detector and the output from the PMT is observed on an oscilloscope. The trace of multiple pulses from the PMT is taken and where the bright edge of the pulses ends is the voltage corresponding to the brightest line of the source. The slope and y-intercept of the simple line, $V_{out} = E_{in}m_1 + b_1$, is found using the two data points.

The next step involves finding the proportionality of the energy thresholds on the electronic boards to incoming voltages. For this, three different threshold values are set at each comparator on an electronics board. This threshold is a voltage that the incoming voltage is compared against. In theory, if the incoming voltage is larger than the comparator voltage then the signal is allowed though and if it is smaller, it is not. However, in practice, there is a range of voltages near the threshold voltage that are partially allowed though. Depending on where the threshold is set, this can be a large or small range.

In order to mimic the voltage of the signal coming out of the PMT from the large plastic dectector, a pulser is used. The settings that best mimic our large plastic response are shown in Table 2.1. The voltages (amplitudes) of the pulses are stepped up to find the range from no signal is allowed through the electronics to the full signal (counting rate) is allowed though the electronics. Using three different comparator thresholds, the line, $V_{threshold-setting} = V_{turn-on}m_2 + b_2$, can be fit using a least-squares fitting algorithm that returns values for m_2 and b_2.

So, the final part is to combine these two pieces of information. If you are trying to set the threshold for a given energy, then the two lines combine to make: $V_{threshold} = (E_{in}m_1+b_1)m_2+b_2$. Where m_1, m_2, b_1, and b_2 were all solved above. If you are attempting to find the energy cutoff for a given, previously set threshold,

Table 2.1: Pulser settings for simulating a PMT signal from the large plastic detector.

Setting	Value
Amplitude	Varied
Base	0 V
Width	40 ns
Delay	5 μs
Lead	15 ns
Trail	20 ns
Period	100 μs

the equation becomes:

$$E_{in} = \frac{V_{threshold} - b_2}{m_1} m_2 - \frac{b_1}{m_1} \tag{2.1}$$

Using this method, it was found that the energy channels of ADELE during the 2009 campaign were different for the top and bottom detectors. Also, channel one was never found since during the 2009 campaign, that channel stopped functioning. After the campaign, hysteresis was added to fix the problem. Therefore, this calibration would not have given the real energy used during the campaign. For the large plastic in the top sensor head, channels 2 through 4 were 284 keV, 948 keV and 4758 keV. For the large bottom detector, channels 2 through 4 were 262 keV, 839 keV and 4158 keV.

2.3.2 Method 2

Another method to calibrate and understand the energy channels of the plastic detectors is by taking data with various gamma ray sources and modeling both the source and the instrument in Monte Carlo simulations. To begin with, three sealed gamma ray sources were used: Barium 133, Cesium 137, and Europium 152. Measurements were taken in the laborartory with the source directly next to the large plastic scintillators and further away, about 20-21 cm radially away. The close data were taken for 6 minutes with 46 minutes of background taken while the far data were taken for 1 hour, with 7 hours and 40 minutes of background taken. Background data are taken either directly before or after the source data are taken but with no sources.

Then the laboratory instrument is modeled as realistically as possible. The simulations were done using GEANT3 (Brun, Carminati & Giani, 1993). Since the instrument was taken apart for upgrades at the time, a new instrument model needed to be made for just the laboratory calibrations. The energy spectrum of each of the sources was modeled in the GEANT3 simulations. Since there is less degeneracy to try to fit the ratio of channels as opposed to each channel separately, the ratios of $\frac{\text{channel 1}}{\text{channel 2}}$ and $\frac{\text{channel 2}}{\text{channel 3}}$ were fit. Barium 133 was used to constrain the $\frac{\text{channel 1}}{\text{channel 2}}$ ratio since most of the gamma rays emitted by Barium 133 are in the range 53 keV-383 keV, which would only fall in channels 1 and 2. Cesium 137 is

also used to fit channel 1 and 2 since the only prominenet gamma ray is at 662 keV, also only falling into channels 1 and 2. Europium 152 is used to fit channel 1, 2 and 3 since the gamma rays in Europium 152 range from 121 keV to 1.8 MeV.

The energy channel thresholds are individually changed in the modeled data until the percent error between the data ratios and model ratios are minimized. Some results of our simulations compared to data are shown in Figures 2.8. However, the best value for channel 1 was unphysical, about 2 keV. In order to understand our simulations, we pushed the densities of the enclosure to extremes. This involved doubling the density of surrounding material, halving that density and making the density 10X greater. Unfortunately, this did not account for the discrepencies that were seen.

Next, we wanted to improve our simulations to make them as realistic as possible. We modeled the plastic box that the sealed source is held in. The thin aluminum enclosure around the plastic scintillator was included in the model. Air between the detector and source was simulated. Since the energy response of the detectors is not perfect because incoming particles lose energy as they pass through the scintillating material and electronics introduce noise, an energy dependent Gaussian convolution of the model spectrum can recreate this effect. We tried different amounts of convolution to simulate this. Also, x-rays from the gamma ray sources were included. Results from these improvements are shown in

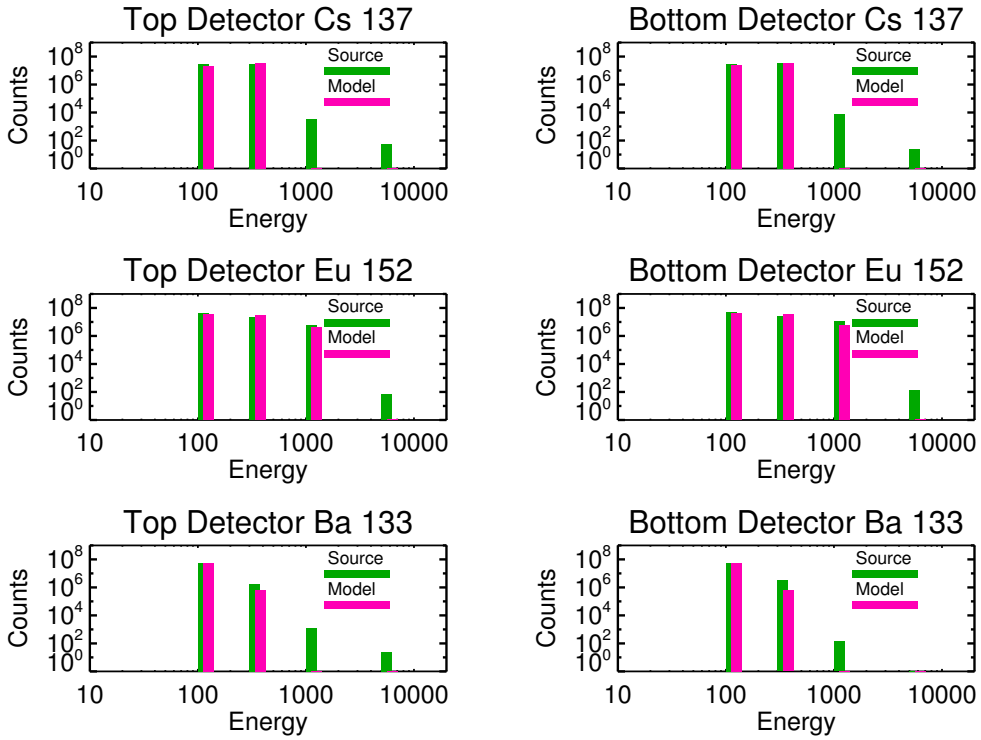


Figure 2.8: Background subtracted, four channel energy spectra for the large plastic detectors in each sensor head compared to a simulated instrument and sources.

Figure 2.9, with a 20% Gaussian convolution. Comparing Figures 2.8 and 2.9, it becomes clear that these improvements did improve the agreement between model and data.

2.3.3 Method Comparison

Method 1 was more reliable than Method 2 and the results from those calibrations were used in subsequent analysis of the ADELE glows. The energy thresholds found using Method 1 were used in modeling of glows, to be discussed in Part II. While Method 1 does introduce human error, Method 2 produced unphysical results for our lowest energy channel.

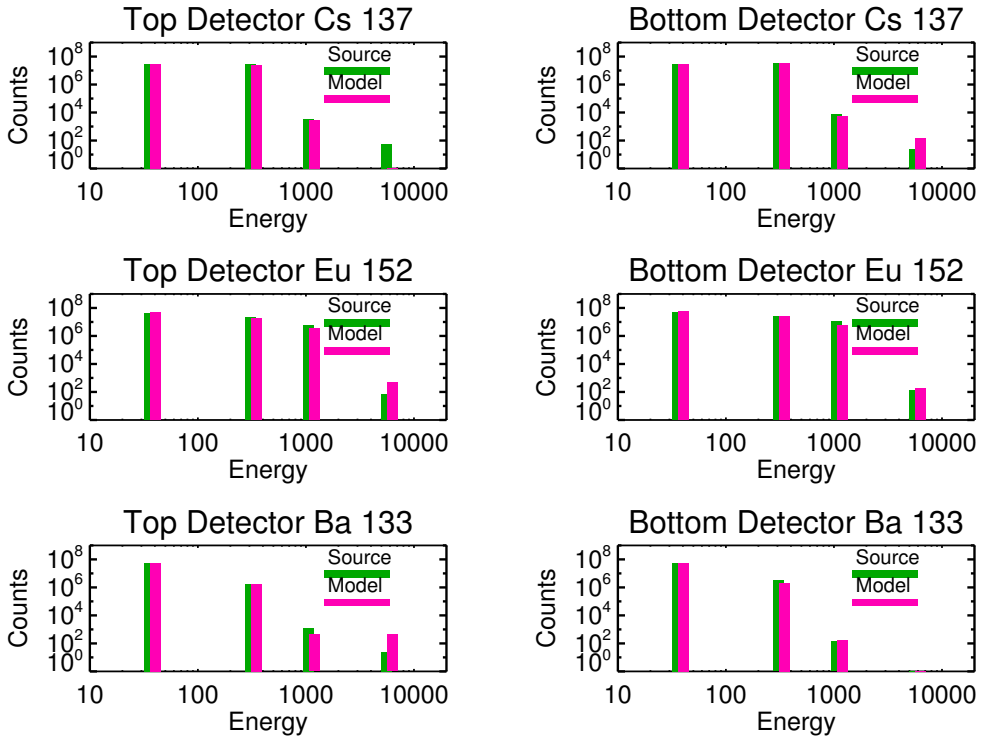


Figure 2.9: Background subtracted, four channel energy spectra for the large plastic detectors in each sensor head compared to a simulated instrument and sources. Simulation includes much more detail, see text

Chapter 3

ADELE Instrument - Version 2.0

In 2013, ADELE was given the opportunity to be a piggyback on the Hurricane and Severe Storm Sentinels (HS3), a NASA mission to study hurricanes with two Global Hawk drones. In order to participate, ADELE needed to be made more compact and be able to both be autonomous and have remote access. These changes caused a complete redesign of the instrument. The following summer, in 2014, ADELE flew on a PS3 with the National Oceanic and Atmospheric Association (NOAA) Hurricane Hunters. In this chapter, the new instrument, along with both HS3 and the Hurricane Hunter campaigns and what was learned will be discussed.

3.1 New Instrument

Starting in 2012, the opportunity to piggyback on the NASA HS3 mission arose. The ADELE instrument was going to be installed on one of the two Global Hawks to be deployed during the campaign. Global Hawks are high-altitude drones built by Northrup Gruman. They can fly up to 18 km high and reach speeds of 575 km/hour. Since this mission was on a drone, ADELE needed to be autonomous. Also, NASA required that a small amount of data be telemetered down at all times to monitor the status of our instrument.

In the new design, the entire instrument was condensed into one box. Greg Bowers, a fellow graduate student, designed the new box and the layout of the instrument. A large 5"X5" plastic, a small 1"X1" plastic and a 3"X3" lathunum bromide ($LaBr_3$) detector were used to maximize space and dynamic range in energy and time. The plastic detectors gave ADELE the ability to count very fast, at least 3 million counts/second for the small plastic detector and possibly higher. The $LaBr_3$ gives ADELE more dynamic range in energy than plastics are capable of.

The detectors are connected to PMTs, powered by high voltage supplies controlled by a sensors services board that is eventually controlled by the computer. The signal from the PMTs is sent to boards that split the signal into four channels. The LaBr3 signal is split into two and sent to two boards so there are eight

energy channels for that detector. The energy thresholds are set via instrument calibration as discussed in Chapter 2, section 2.3, sub-section 2.3.1. The signals from the board are then sent to the FPGA where counts and deadtimes are binned into 50 μs rates and then sent to the computer. The FPGA is a Virtex 6 board, programmed by undergraduate Cody Harris.

The PMT voltages can be set by the computer, except for the $LaBr_3$ PMT, whose voltage can be adjusted manually. The voltages are controlled and measured through the use of analog to digital and digital to analog converters through a Measurement Computing USB box. The two USB boxes in the previous instrument have been condensed to one box. In addition to voltage controls and monitor, the USB box also measures temperatures from around the instrument. To make the most of the four analog inputs, a multiplexer on the service sensor board is used, that switches between various measurements. The multiplexer is controlled by a digital hexadecimal code sent by the computer via the USB box. The box is controlled by the computer though a C driver written by Dr. Warren Jasper of North Carolina State University.

The software was written in C on a single board computer running Linux. Multithreading was implemented to take advantage of the computer's two cores; one core is used to capture packets of data from the FGPA every 50 μs and bundle them into 20 ms blocks (the slave thread) while the master thread on the other

core writes the data to disk, sets the voltages, monitors and records temperatures and voltages, sends telemetry data and receives commands from the ground. Two 512 GB SSD drives were mirrored for redundancy in case of file corruption.

The Global Hawk can fly up to 18 km in altitude and while ADELE was going to be installed in an environmentally controlled compartment, this was still at 8 km altitude equivalent pressure. The high voltages were potted to prevent arcing at these altitudes.

The ADELE instrument generates a lot of heat. The computer and FPGA both have small fans on their processors, but at high elevation, fans become much less efficient as there is less air. But it is also much cooler at high elevation, so cooling becomes less important. However, ADELE would be on the tarmac in both the desert of California and near the coast in Virginia, both in summer, so to be safe, a large fan on the exterior of box near the FPGA and computer was installed with a hole on the opposite end of the instrument box to help circulate air through the entire system.

3.2 HS3 Mission

The Hurricane and Severe Storm Sentinel (HS3) is a 5-year NASA mission. The primary goals of the mission are to understand hurricane initiation and intensification by understanding the large-scale environment and smaller-scale internal

processes. To achieve this, two NASA Global Hawks were used, one to fly over the areas surrounding the hurricanes (environmental) and one flying over the hurricane (over storm). ADELE was installed on the over storm plane. Installation occurred at NASA Dryden Flight Research Center (DRFC) on Edwards Air Force Base near Lancaster, CA, while flights were based out of NASA Wallops Flight Test Facility on Wallops Island, VA.

3.2.1 Testing

NASA required all instruments to pass environmental testing at DRFC. This consisted of vibration testing and thermal/vacuum testing. For the vibration tests, accelerometers were placed all over the instrument. Figure 3.1 and Figure 3.2 show the lowest energy channel on each detector during two of the vibration testings, lateral and inline vibrations. There was a lot of noise induced in the detectors during testing, specifically the large plastic and small plastic. This noise was an issue throughout the flights although it was the worst during testing.

During the thermal and vacuum test, the instrument was first taken down to 32° F and stayed at that temperature for 15 minutes while running. Then the instrument was turned off and brought down to -40° F and to an atmosphere equivalent to 28 kft for 15 minutes. Then the instrument was brought back to sea level pressure and 131° F for 15 minutes. After 15 minutes, ADELE was turned

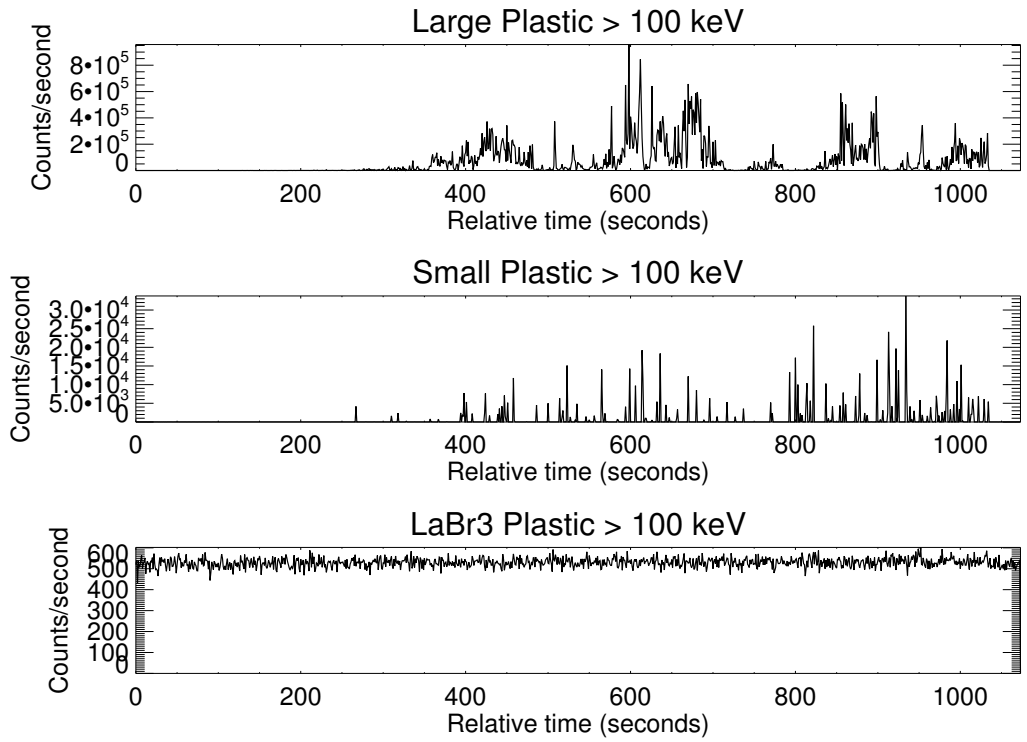


Figure 3.1: The lowest energy channel (>100 keV) count rates for the three ADELE detectors: large plastic, small plastic, and a $LaBr_3$ detector during lateral vibration testing (side to side shaking).

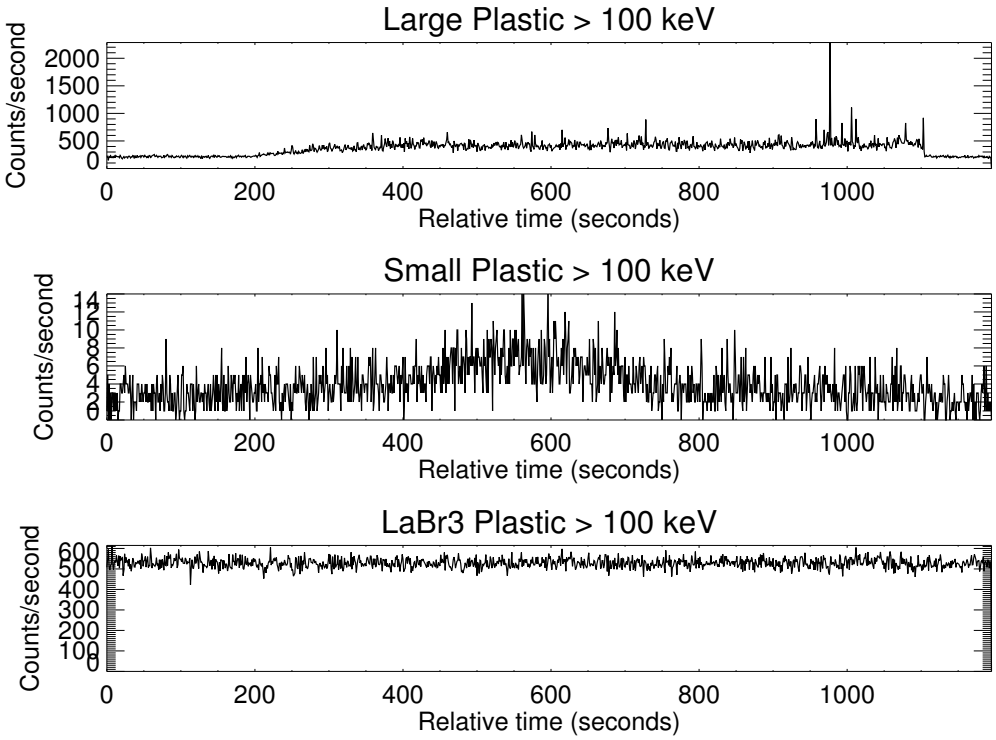


Figure 3.2: The lowest energy channel (>100 keV) count rates for the three ADELE detectors: large plastic, small plastic, and a $LaBr_3$ detector during the inline vibration testing (front to back shaking).

back on at 131° F and performed well. Then ADELE was turned off and brought to 160° F for 15 minutes. After, ADELE was brought back to room temperature of 77° F and still performed normally. Both vibration and thermal/vacuum tests were passed so ADELE was then ready for integration.

3.2.2 Integration

After testing was passed, ADELE was installed onto the plane. This was followed by a series of integration tests to make sure all instruments were not interfering with each other. The ADELE installation was more than a physical installation; it also required ADELE's data to be incorporated into the Global Hawk data stream so it could be telemetered to the ground. There were two types of telemetry being used, an Iridium satellite connection that allowed ADELE to send user packets and status packets via the NASA Airborne Science Data Acquisition and Telemetry system (NASDAT). The status packets were required by NASA and contained our instrument timestamp, voltage monitors, computer and FPGA temperatures, and a few count rates. These were combined with other instruments' status packets and sent to the ground every second. Every 10 seconds, ADELE sent another packet with the rest of the count rates and temperatures via the user packet connection. This packet was only sent to the NASA-provided ADELE computer station on the ground.

An external GPS pulse per second was provided by the Global Hawk. This is pulse is required for our FPGA to take data and is used for it to keep track of time. The ADELE computer used the NTP server aboard the Global Hawk to get its time. As long as the computer time is accurate to within one-half of a second when synced with the FPGA at instrument start-up, the FPGA would continue to keep accurate time to sub-/*mu*s resolution.

3.2.3 Mission

From NASA Wallops, ADELE had the opportunity to fly on four science flights between September 3 and September 17. One of these flights was cut short due to a navigation system failure. The reason for the small number of flights was that 2013 was a very slow hurricane season, with only two tropical storms becoming hurricanes. Another reason is there were many technical and mechanical issues with the plane. Many flights would get cancelled before the plane ever took off.

Unfortunately, in addition to very few flights, on the flights ADELE did participate in, the plane never flew within 10 km of any lightning. This was due to both lack of lightning and caution taken by the pilots to avoid overshooting cloud tops. This meant that ADELE measured no high-energy radiation from thunderstorms or lightning. This campaign was very valuable, however, because it taught us how our instrument could be improved. There was a significant noise

problem in the large plastic detector and a smaller noise problem with the $LaBr_3$. We also learned about the drawbacks of only syncing the FPGA to the computer time at start-up. If the computer does not have a valid time at start-up, as was the issue on a couple of flights, then the FPGA time will be off for the rest of the flight.

3.3 Hurricane Hunters

At time of writing, data from the 2014 hurricane season was still being searched for interesting results. There were no ADELE results from the first few flights but it is possible that something of interest could still be found. The flights and integration took place at the NOAA Flight Operations Center on MacDill Air Force Base in Tampa, Florida. ADELE was installed onto one of two Orion P3s used by the Hurricane Hunters. Figure 3.3 shows photos of the plane, NOAA 42, nicknamed Kermit.

There were relatively few changes between the 2013 HS3 campaign and the 2014 Hurricane Hunter campaign. The main improvement was to deal with the noise issue observed during the 2013 campaign. To help deal with this problem, hysteresis on the front end boards was added. The noise was due to after pulsing in the detectors. The hysteresis required that an incoming peak pass between two voltages before they would be processed, thereby reducing the effect of the



Figure 3.3: NOAA 42, nicknamed Kermit. One of two Orion P3s used by the Hurricane Hunters to chase hurricanes.

noise from after pulsing. After the hysteresis was added, the instrument was recalibrated to set the energy channel thresholds.

Although the Orion P3s are manned by both pilots and scientists, ADELE did not have an operator on the flights. This meant that the instrument needed to be fully autonomous. All the telemetry was disabled. Since this mission was much more hands-off, data were configured to write onto the two hard drives sequentially, lowering the rate of changing hard drives by two. For instrument status, an LED light was added. The software turns the light on when the instrument is functioning correctly and routinely checks count rates and voltage monitors to determine instrument health. If anything is amiss, the light turns off. In the 2013 software, ADELE could be soft powered down by a command from the ground. In the new version, a soft power down switch was added. When pushed, all the high voltages on the PMTs are ramped down and the computer is soft powered down. A hard power down switch was also added. This is to be pushed after the instrument finishes its soft power down, and it mechanically cuts power to the instrument.

Integration with NOAA was a very seamless process. I think we learned a lot from the 2013 campaign that made us much more prepared for the 2014 integration. The one concern was about vibration on the P3, since the plane penetrates storms. So far, this has been a very minor issue.

Part II

Gamma Ray Glow Measurements

Chapter 4

The ADELE Glows

4.1 Introduction

Gamma-ray glows are long duration emission of x-rays and gamma rays coming from thunderstorms. In the summer of 2009, ADELE observed 12 gamma-ray glows while flying on the National Center for Atmospheric Research (NCAR) Gulfstream V. Previously the only glows observed on a plane were the first glows ever discovered, the glows measured by McCarthy and Parks during their flights on a NASA F-106 jet in the 1980s (McCarthy & Parks, 1985; Parks et al., 1981). The detectors flown on these flights were only sensitive to x-rays up to 110 keV. Since then glows have also been measured by balloon (Eack et al., 2000, 1996a,b) and from ground stations (Tsuchiya et al., 2007; Torii et al., 2009; Brunetti et al.,

2000; Chilingarian et al., 2010; Chubenko et al., 2000; Gurevich et al., 2011a).

Gamma-ray glows are sustained gamma ray emission from relativistic runaway electron avalanches (RREA) (Torii, Takeishi & Hosono, 2002; Tsuchiya et al., 2007; Babich et al., 2010). They have been measured from several seconds to several tens of minutes (Torii et al., 2009). There are a few instances of lightning terminating the glows (Tsuchiya et al., 2007; McCarthy & Parks, 1985). The McCarthy and Park termination looks extraordinarily similar to the brightest ADELE glow, which was also abruptly terminated, although no lightning sferic was detected by ground sensors. Figure 4.1 shows the McCarthy and Parks glow compared to the brightest ADELE glow. Two of the three peaks before the ADELE glow are positron annihilation lines at 511 keV, which is most likely due to the plane discharging itself. It is possible that the peak before the McCarthy and Park glow is also due to positrons. The reason for the larger amplitude of this first peak in the McCarthy and Park data could be because their instrument was much more sensitive to the direct measurement of positrons. Their insturment included a much thinner scintillator that was external to the airplane so positrons were likely to be stopped directly in their detector. The ADELE instrument was inside the plane, inside Al sensor heads so it was more sensitive to the gamma rays from the annihilation of positrons with electons, and would have detected a much weaker signal, as seen in the data. The last similarity between the two sets

of data is the overall decrease in the glow intensity with a slight "second bump" before termination.

4.2 Interpreting the ADELE Results

In order to understand the ADELE data better, we can use both the hardness ratio and top/bottom ratio. The hardness ratio and top/bottom ratio varies for each glow. The hardness is a measure of how many high energy photons there are compared to lower energy ones. A higher hardness ratio implies a harder spectrum with relatively more high-energy counts compared to a softer spectrum. Hardness, in the case of glows, can imply that less spectral imformation has been lost. The further away from a source, the softer the spectrum will get. This is due to Compton scattering of photons on their way to the detector. The Compton scattering softens the RREA spectrum. This can be seen in Figure 4.2. The bottom panel shows the spectral ratio, $\frac{\text{channel 2}-\text{channel 3}}{\text{channel 3}}$, for the ADELE instrument's sensitivity to a TGF. The TGF spectrum is the same as a glow, but the glow is much less intense, so it is most likely not detectable from 10 km away. This figure shows that the hardest spectral ratio, in this case a lower number, would result directly above or below the glow. The reason that this is the case. If the instrument is directly above an upward directed glow then ADELE would be measuring the electrons and the associated gammas before they have Compton scattered. If

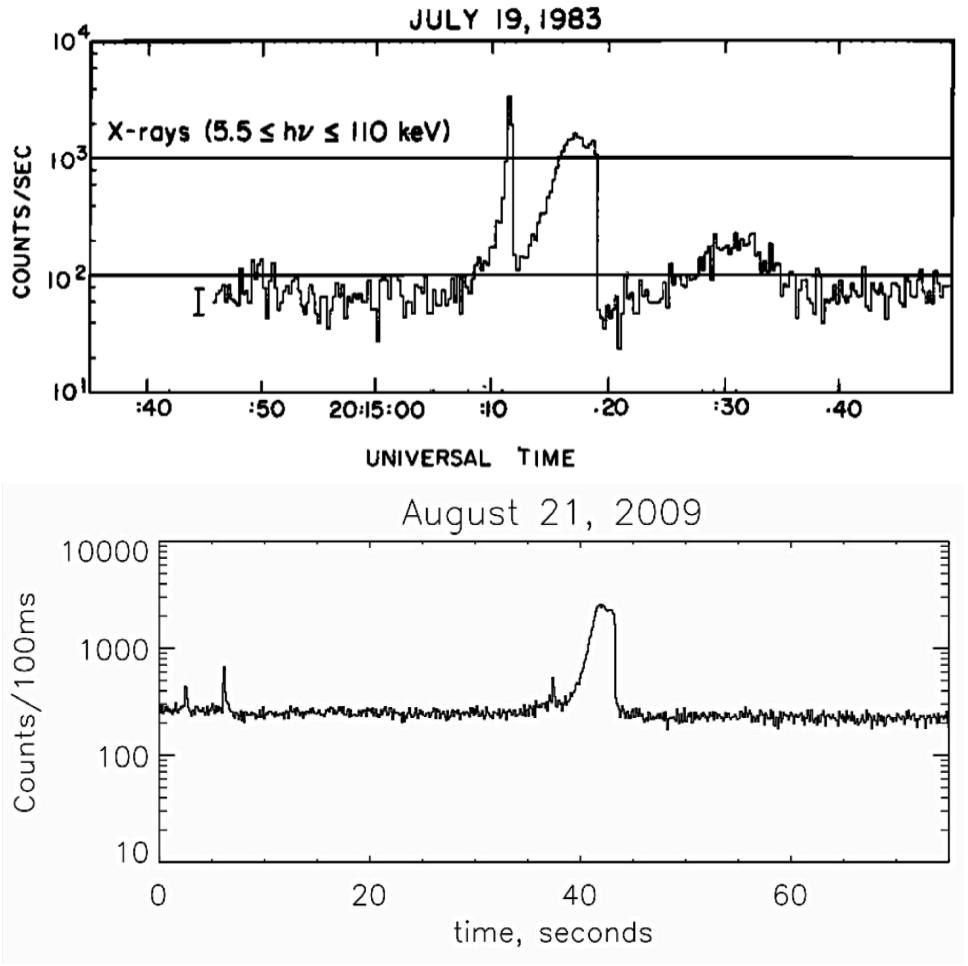


Figure 4.1: Top: From (McCarthy & Parks, 1985). A glow that is abruptly terminated by lightning. Bottom: The brightest ADELE glow on August 21. There was no detected lightning during the abrupt termination.

ADELE is below an upward facing glow, the spectrum will still be harder because then ADELE us measuring the radiation from the positrons traveling downward, although the detected radiation would be much less than that of the case where ADELE is measuring radiation from the electrons.

Top/bottom ratios give directionality. A uniform top/bottom ratio implies distance away from the RREA source or that ADELE is directly to the side of the glow, so the directionality information has been Compton scattered away as the radiation passed though more air on the way to the ADELE detectors. A top/bottom ratio higher than unity implies most radiation coming from above, so flying below a RREA region, or through downward directed RREA, while a ratio less than unity implies the opposite geometry. The top plot in Figure 4.2 shows that the best directionality information is seen above and below the RREA, as would be expected.

4.3 Overview of the ADELE Glows

With the exception of one glow, all of the ADELE glows were seen on flights out of Melbourne, Florida, with the other glow seen on a flight out of Broomfield, Colorado. These glows were observed on 7 of the 9 ADELE flights. The ADELE glows range from 4 to 112 seconds. For all the glows, except the brightest, the duration of the glow was consistent with the motion of the Gulfstream V moving

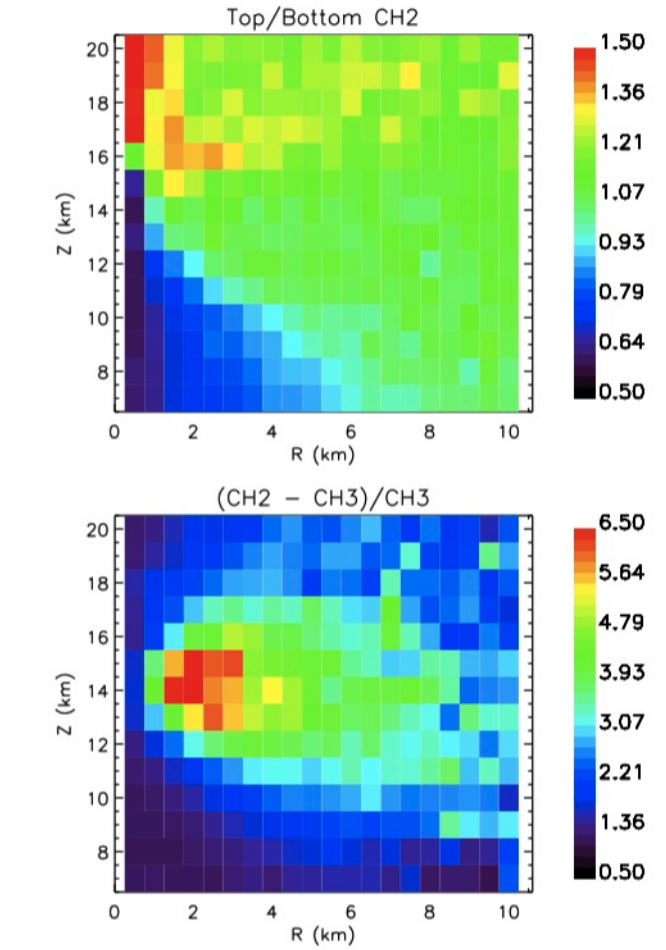


Figure 4.2: Top: The expected top/bottom ratio from a TGF at various altitudes as a function of distance from ADELE. ADELE is located at 14 km altitude. Bottom: The spectral ratio from a TGF. TGFs have the same spectrum as glows but are much brighter.

past a stationary RREA cell. ADELE glows were seen 11 out of the 149 times that the Gulfstream V passed near an active lightning cell, making them an order of magnitude more common than TGFs (Smith et al., 2011b).

The brightest glow on August 21, 2009 will be discussed briefly here but will be discussed in much more detail in Chapter 5. This glow was analyzed and modeled more carefully than the other glows because it was 20 times brighter than any other glow and has much better spectral information. For this glow, ADELE flew directly through downward facing RREA. The other glows were most likely viewed from either above or to the side of the active RREA cell. Figures 4.3 and 4.4 shows the time profile for each glow with the each channel plotted. Counts per second in the summed large plastic detectors for each differential energy channel is shown: 50-300 keV, 300-1000 keV, 1-5 MeV and > 5 MeV. The background has been subtracted, altitude corrections made, and for the lowest energy channel, 50-300 keV, the count rate has been divided by 3 to let the higher energy channels have more prominence in the plot. All the glows are different durations and have different count rates in each channel, some with very few counts above background in the higher energy channels.

There are two glows on August 31 with double peaks, possibly three. August 31, 2009 D is from the flying by the same glow region twice. This is only counted as one glow because it is two measurements of the same glow. For August 31,

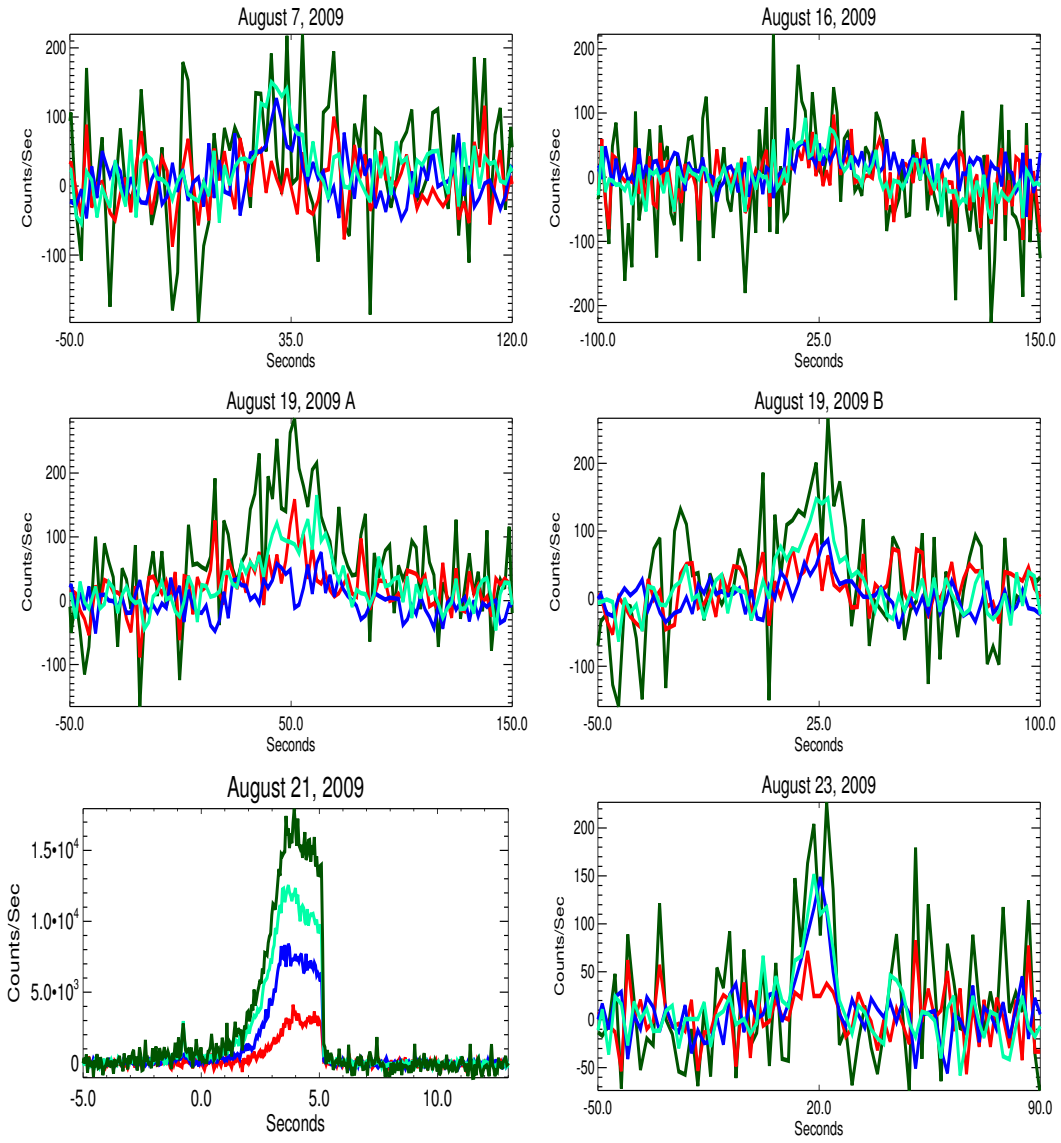


Figure 4.3: Counts per second in the four differential energy channels of the ADELE instrument during the 6/12 glows. The dark green line is 50-300 keV (count rate divided by 3), the turquoise line is 300-1000 keV, the blue line is 1-5 MeV and the red line is >5 MeV.

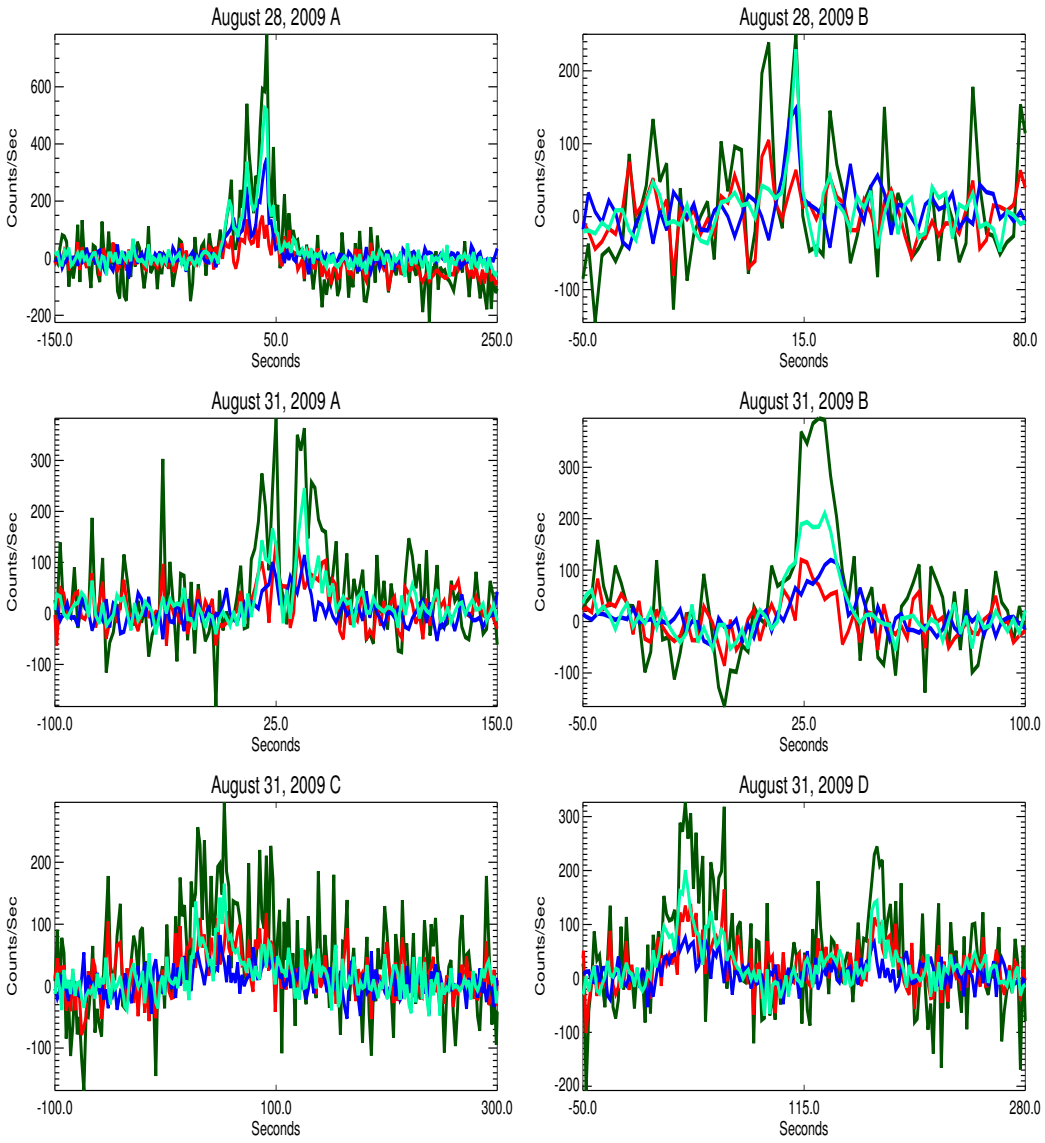


Figure 4.4: Counts per second in the four differential energy channels of the ADELE instrument during the 6/12 glows. The dark green line is 50-300 keV (count rate divided by 3), the turquoise line is 300-1000 keV, the blue line is 1-5 MeV and the red line is >5 MeV.

2009 D, analysis for top/bottom ratio and hardness ratios of the glow are done twice, since the time between the glows is more than a minute. The other double peaked glow is August 31, 2009 B. This glow is not from flying by the same glow twice. Since the glows are so close together it is possible that the glow turned on or off or they were from very two close cells. Since the two peaks are so close together in time, the hardness and top/bottom ratio are only calculated once for the two peaks. It is possible that there is a very weak second glow during August 31, 2009 C. These double-peaked glows will be discussed further in Section 4.4.

Table 4.1 shows the duration for each glow in seconds and the distance to the active lightning nearby in kilometers (to be discussed later in Section 4.4), along with the top/bottom ratio and the hardness ratio. The top/bottom ratio is for integral channel 2 (>300 keV). The hardness ratio shown is $\frac{\text{channel 3}}{\text{channel 2}-\text{channel 3}}$, or $\frac{>1 \text{ MeV}}{300 \text{ keV}-1 \text{ MeV}}$, where larger numbers imply harder ratios now. To calculate both the top/bottom and hardness ratios, the counts were first background subtracted and corrected for altitude fluctuations, discussed below.

The gamma-ray background changes as a function of altitude. Close to the ground, radiation comes from both the ground and the cosmic-ray background. As altitude increases, the cosmic-ray background increases, as there is less attenuation from air but the radiation from the ground decreases. There exists a background minimum, when increasing in altitude on an airplane. After this point, as altitude

Table 4.1: ADELE Glows

Date	Duration(s)	Distance(km)	Top/Bottom>300 keV	Hardness
080709	18	na	0.61	0.82
081609	93	1.11	0.87	1.36
081909a	76	4.78	0.57	0.99
081909b	24	0.45	0.60	0.71
082109	5	0.56	1.74	0.83
082309	4	0.66	0.95	1.14
082809a	70	0.63	0.75	1.03
082809b	4	0.61	0.85	1.16
083109a	46	0.85	1.14	1.24
083109b	38	0.92	0.91	0.89
083109c	112	0.81	1.14	1.42
083109d1	63	0.75	0.63	1.16
083109d2	28	0.03	0.76	0.94

is increased, the radiation background increases as a function of altitude. To remove this effect of altitude fluctuations, a linear fit was found during the take-off of each flight, from 10 km to cruising altitude. This effect was then subtracted from the data. It ended up being a very small effect, but served as proof that glows were not fluctuations in the background from altitude.

Figure 4.5 shows the relationship between the top/bottom and hardness ratio. After the very bright glow on August 21, that has a very high top/bottom ratio, has been removed, a linear relationship can be found between these ratios. The Pearson correlation coefficient for this relationship is 0.69 with a one-tailed probability of 99.36% that this number is not random. This linearity implies that the hardness ratio increases with increasing top/bottom ratio. Figure 4.2

implies that harder spectra will have either top/bottom ratios further from unity. Since ADELE was most likely flying above the glows, given by the top/bottom ratios and the altitude the Gulfstream V was flying in relation to charge centers of thunderclouds, this linearity comes from the fact that harder glows will have more penetrating radiation. This penetrating radiation will be more likely to be detected by the top detector, explaining the increasing top/bottom ratio.

Figure 4.6 looks at the hardness ratio for the top and bottom large plastic detectors separately. The Pearson correlation coefficient is 0.44 with a 6.49% chance that number is random. This tells us that there is no real correlation between the hardness ratios in the seperate sensor heads.

4.4 Glows and their relationship to lightning

Lightning is a very good indicator of electrified storms however storms can be electrified without any lightning activity (MacGorman & Rust, 1998). Also, glows may be an indication of an electrified storm where lightning activity has been diminished (Tsuchiya et al., 2013). Babich et al. suggests that RREA growth can lead to the development of lightning (Babich et al., 2012). However, for purposes of this analysis, we use lightning as a trace for the electrified cell. In order to do this, we used the lightning activity nearby as reported from three lightning networks: the United States Precision Lightning Network (USPLN), Weatherbug

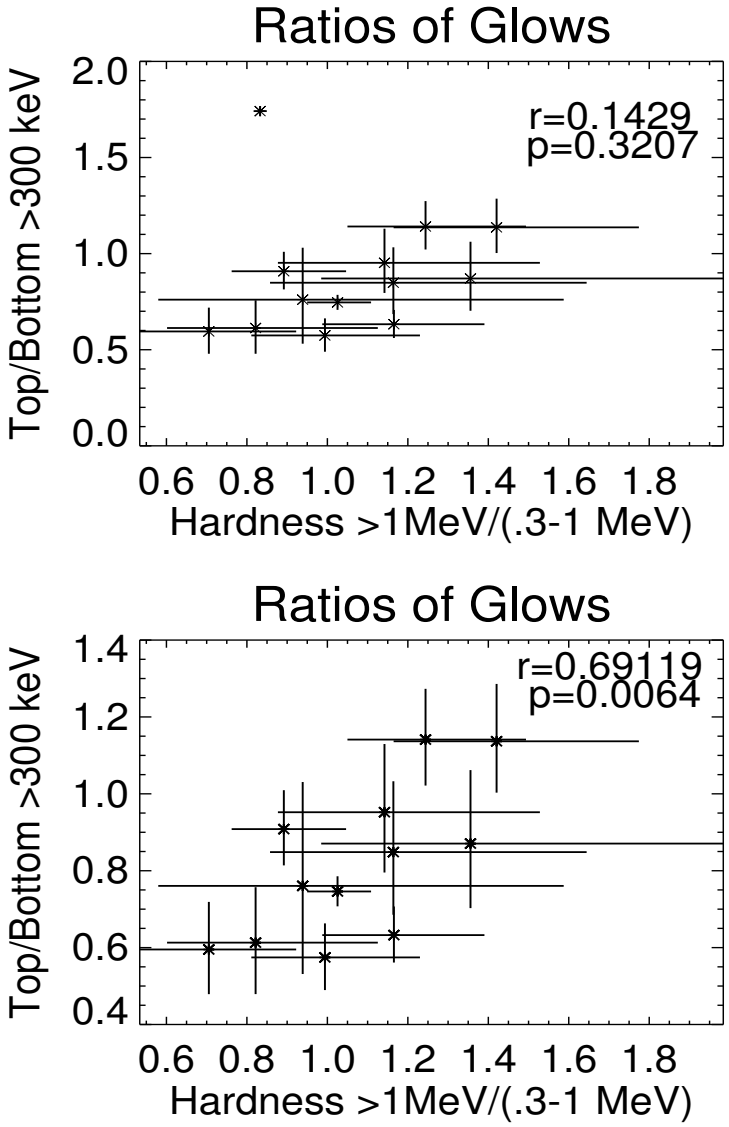


Figure 4.5: The hardness versus top/bottom ratios for the ADELE glows. The top plot includes all glows while the bottom plot is after the brightest glow on August 21 has been removed

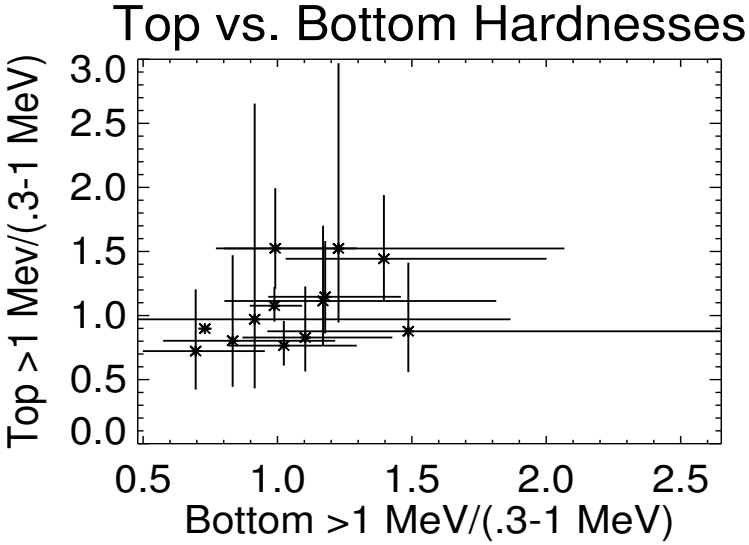


Figure 4.6: The hardness ratio in the bottom large plastic detector versus the hardness ratio in the top detector.

Total Lightning Network (WTLN), and the National Lightning Detection Network (NLDN). Figure 4.7 shows the lightning activity within ±5 minutes and 50 km of each glow. These plots only show USPLN lightning data because it was the only network where we had lightning data both temporally and spatially away from the plane's trajectory. The line is the flight trajectory of the Gulfstream V while the red portion of the line is where ADELE was when the glow was measured.

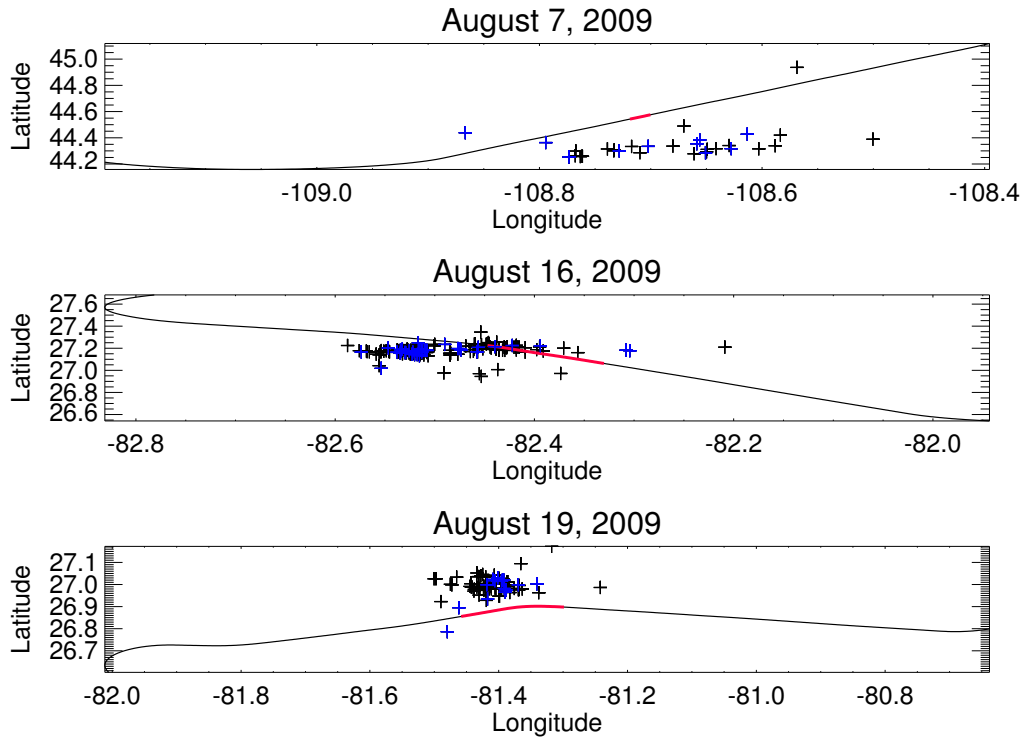


Figure 4.7: The nearby lightning activity to three of the ADELE glows. The cross marks are USPLN lightning within ±5 minutes and 50 km of the glow. The black path is the Gulfstream V trajectory ± 5 minutes of the glow. The red line is the plane's path during the glow. The blue cross marks are lightning within ± 30 seconds of the glow.

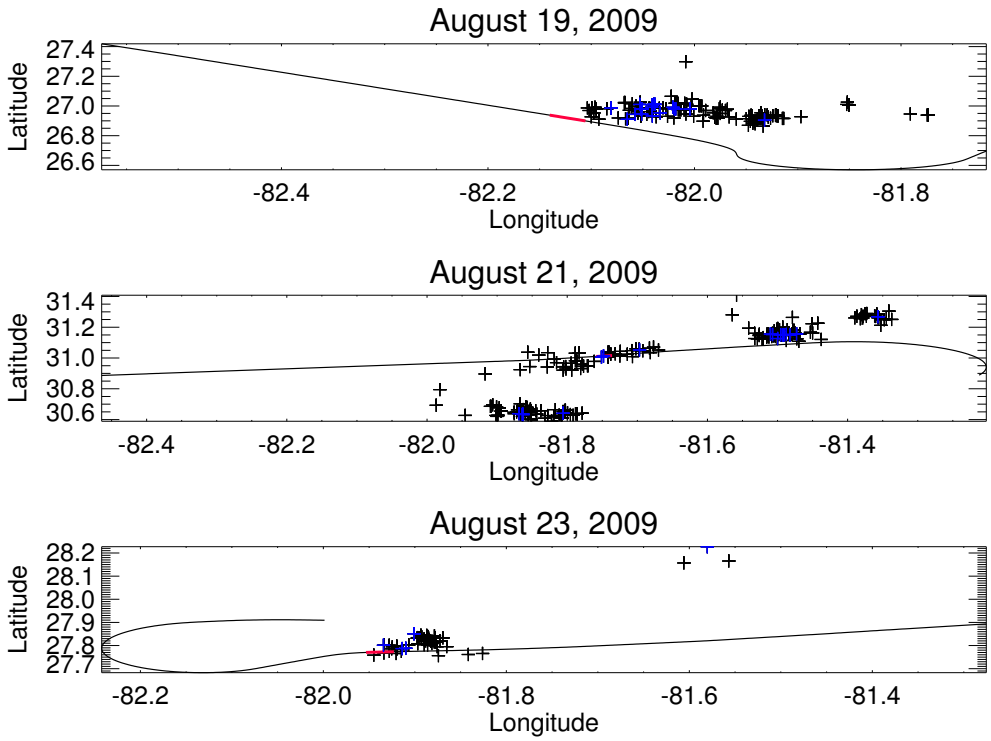


Figure 4.7 continued

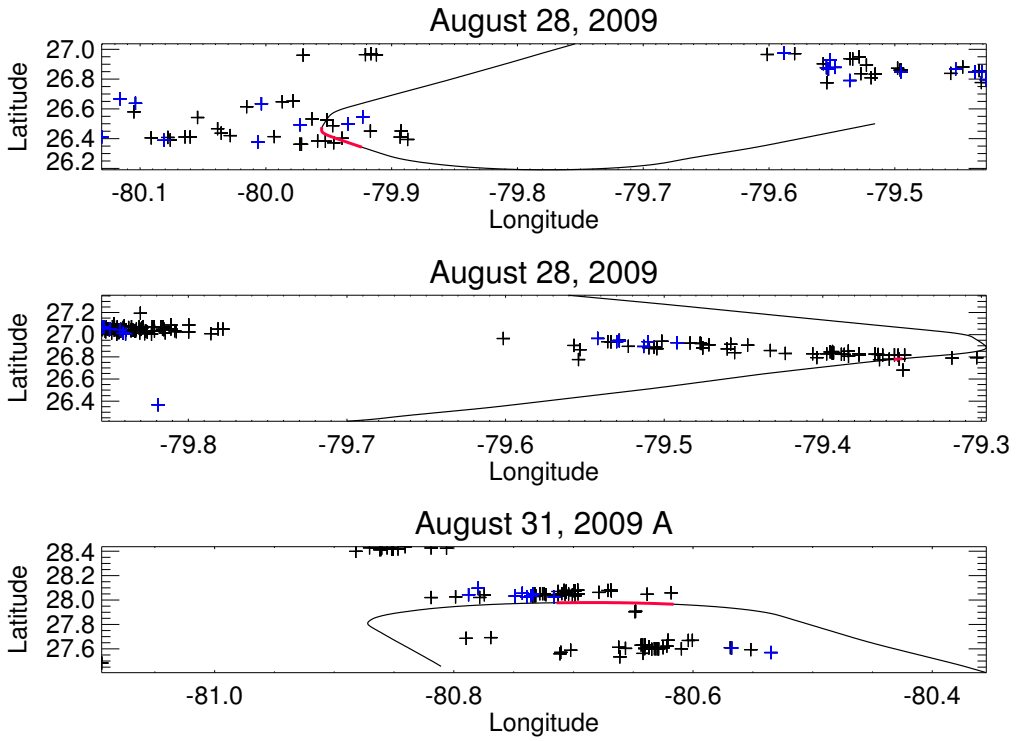


Figure 4.7 continued

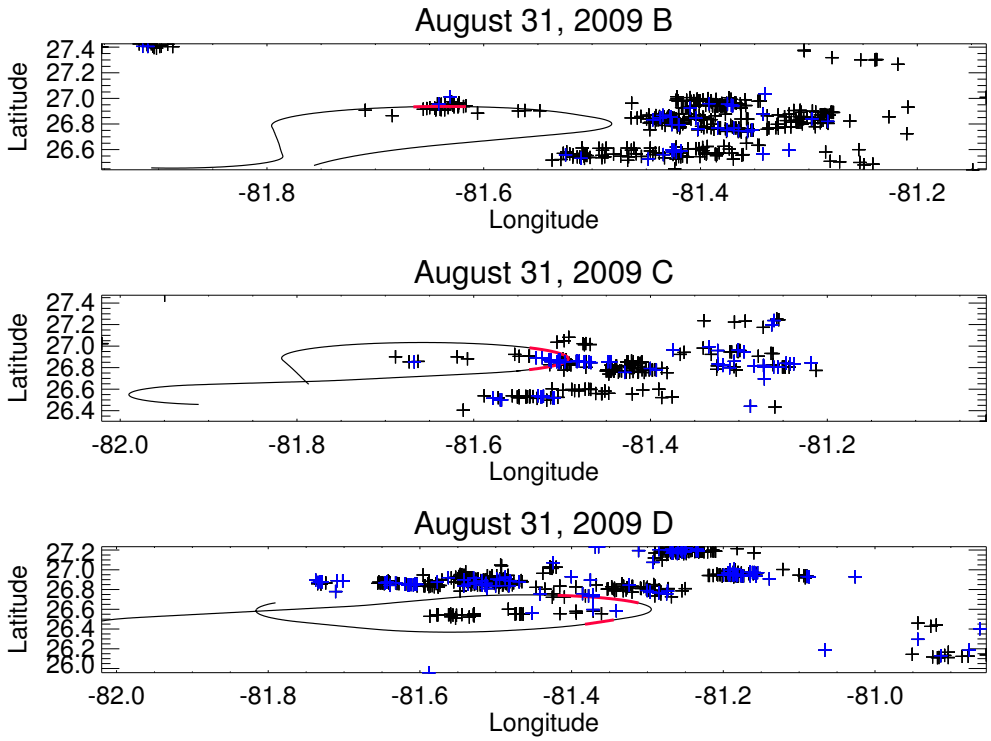


Figure 4.7 continued

Of interest in Figure 4.7 is the glow on August 7, 2009. This was the only glow observed on the flights out of Colorado. There is no lightning activity within 32 km of the instument at any moment. The lightning that is shown nearby to the Gulfstream V trajectory is lightning that occured either before or after the plane was there. This is the only glow where this is the case.

For glow August 31, 2009 D we flew by the same cell twice and referencing back to Figure 4.4, we can see a double peaked glow. This mean that this glow could have lasted as long as 185 seconds. It is possible that glow August 31, 2009 C has a double peak from flying through the same glow region twice, as is noticeable in the turn in the flight trajectory in Figure 4.7. The double peaked glow August 31, 2009 A does not appear to be flying by the same region twice during the glow. It is possible that we are measuring two different glow cells here.

4.4.1 The Glow Lightning Model

In order to understand the glow intensity as a function a distance, a two-staged Monte Carlo simulation was used. In the first stage, RREA approaching relativistic feedback was fully modeled in Dwyer (2003, 2007). The second stage was propagating the gamma rays from stage 1 through the atmosphere, using the same method discussed in Smith et al. (2010). The output glow intensity as a function of radial distance from the Monte Carlo simulations were fit using both

an exponential and Gaussian function as shown in Equation 4.1. This function is convolved with lightning data to find the relationship of distance to lightning and expected glow intensity.

$$E(t) = e^{\frac{-d_f(t)}{d_0}} + Ae^{\frac{-d_f^2}{2\sigma^2}} \tag{4.1}$$

Where $E(t)$ is the expected counts in arbitrary units as a function of time and $d_f(t)$ is the distance of the flash to the the plane at a given time. Using a non-linear least squares fitting algorithm, mpfit (Markwardt, 2009), the variables A, σ and d_0 were found to be 2.0593, 0.6971, and 0.6591.

Then each lightning flash was convolved with Equation 4.1, to find a simulated or expected count rate depending on the distance to an electrified cell. Figure 4.8 shows the expected count rate over the real count rate. The lightning convolution is not exact, it does not get the glow amplitude correct, but it does predict all but the one glow in Colorado that had no lightning activity anywhere nearby. The expected counts also over predicts glows. In fact, glows were only observed 11 out of the 149 times there was a peak in the expected counts. Figure 4.9 shows the peak expected counts versus the real glow peak count rate. The glow 080709 is the only glow with no lightning activity nearby and thus has a zero peak model value. Also of interest is glow 081909a, which has almost a zero peak model value. The value is 0.01 so there is very little lightning activity nearby. Glow 082809a is the second brightest glow after glow 082109, which is not shown. Glow 082109

has a peak data value of 22786 and a peak model value of 33.58. Both 082809a and 082109 show that the model is not very good at predicuting intensity. Glow 083109c has a lot of nearby lightning activity yet the glow was not very bright.

We can also use the expected counts model to determine a distance from ADELE to the glow. This is done by taking the weighted mean of the distance to the flashes, where the weight is Equation 4.1. The distance can be calculated as a function of time as $d(t) = \frac{\sum d_f(t)E(t)}{\sum E(t)}$, where $d_f(t)$ is the distance from the plane to a flash at a given time. From this, we can look at how distance away can affect glow parameters. Figures 4.11 and 4.10 showed how the top/bottom ratio and hardness ratios changed as a function of distance. Both plots in Figure 4.10 do not show the glow on August 7; since there is no lightning nearby, a distance cannot be calculated. Also, the first glow on August 19 has also been removed from the bottom plot. This glow is 4.78 km away, more than 3 times further than any other glow. This glow may be another example, like the glow on August 7, where gamma rays are being measured from an electrified cell that does not produce lightning. This glow also had a very small peak model value in Figure 4.9. The Pearson correlation coefficient for the bottom plot in Figure 4.10 is 0.57 with a 3.43% probability that this result is random. Figure 4.11 has the glow on August 7 removed from both plots since no distance can be calculated. The glow on August 19th has been removed from the bottom plot for the same reasons

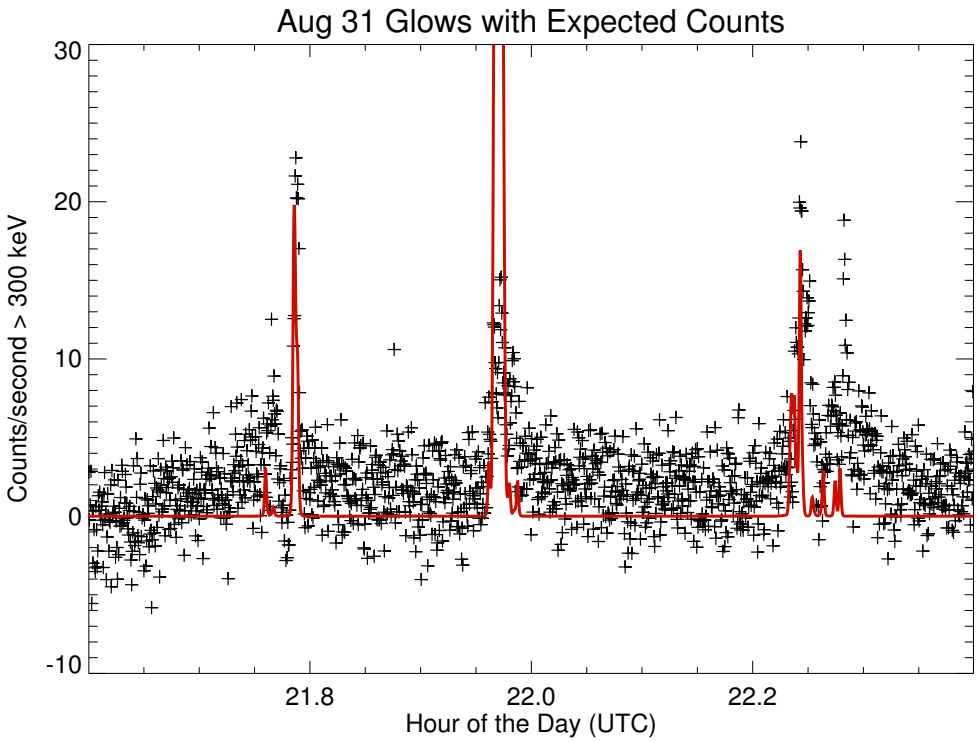


Figure 4.8: The red curve is the expected counts model as a function of time. The black crosses are the summed, background subtracted counts in the two large plastic detectors.

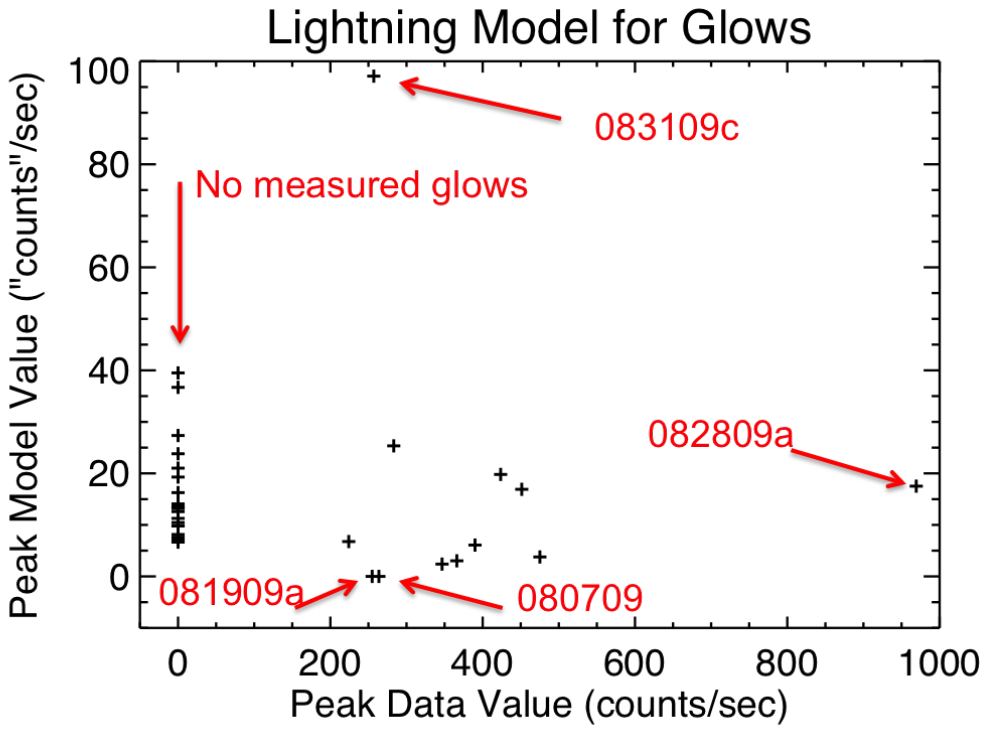


Figure 4.9: The peak count/second rate for each glow in the >300 keV summed large plastic detectors versus the peak in the expected count model. The glow on August 21 has been removed from the plot to show the other glows more clearly.

as in Figure 4.10. The glow with the very high top/bottom ratio is the glow on August 21 and the reason for this high ratio is because ADELE was directly in the end of the avalanche and was mainly measuring electrons. This will be discussed further in Chapter 5. Even when the August 21 glow is removed, there is no likely correlation between distance and top/bottom ratios. Both Figures 4.10 and 4.11 are consistent with Figure 4.2.

The duration of the glow should also change depending on how close they were measured. If a glow is very close, you expect it to be shorter in duration because the instrument spends less time in its closest approach to the glow. Figures 4.12 shows the relationship between distance and glow duration. The duration was found by taking the second moment of the summed large plastic Channel 2 ($>$ 300 keV) counts. The top plot in Figure 4.12 has all glows shown except for the glow on August 7, since no distance can be found. The bottom plot in Figure 4.12 has the the outlier, the first glow on August 19, removed. This glow is most likely not associated with an active lightning region. When this outlier is removed, there is a linear relationship as expected. The Pearson correlation coefficient is 0.61423 with a 2.22% probability that this is random. It would also be expected that the glow peak intensity would be inversely related to the glow distance. However no linearity is found, even when several outliers are removed. This implies that glow intensity is an intrinsic property to the glow and not a geometrical parameter.

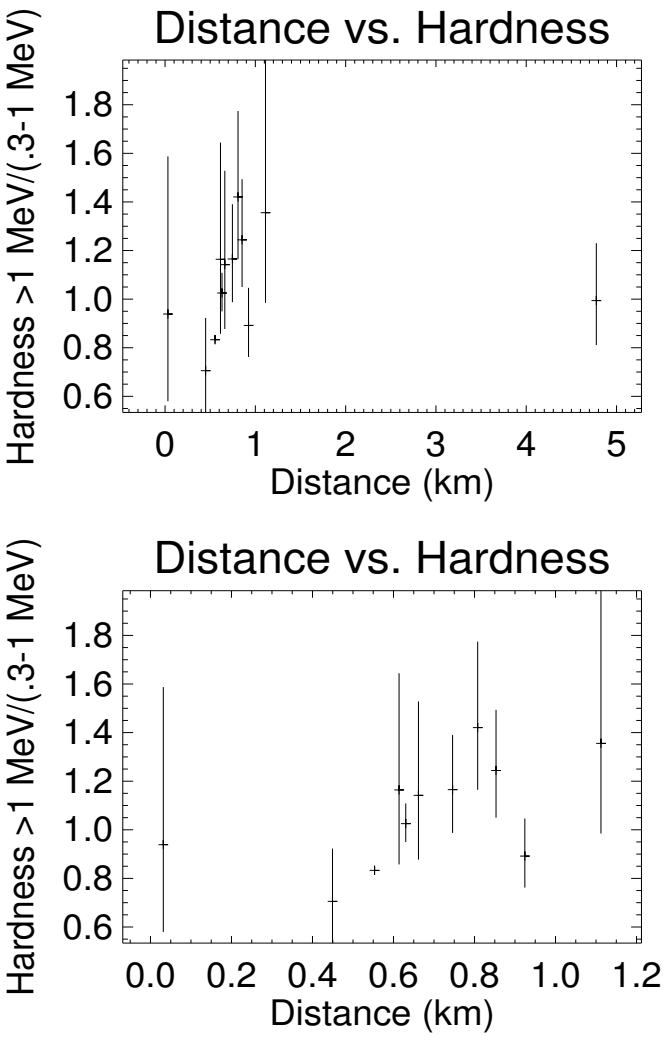


Figure 4.10: The glow hardness $\frac{\text{channel 3}}{\text{channel 2}-\text{channel 3}}$ as a function of distance from an electrified cell. The top plot has all glows except for the glow on August 7 because no distance can be found for that glow since there is no lightning activity nearby. The bottom plot has the glow on August 7 and the first glow on August 19 removed (the outlier at 4.78 km in the top plot).

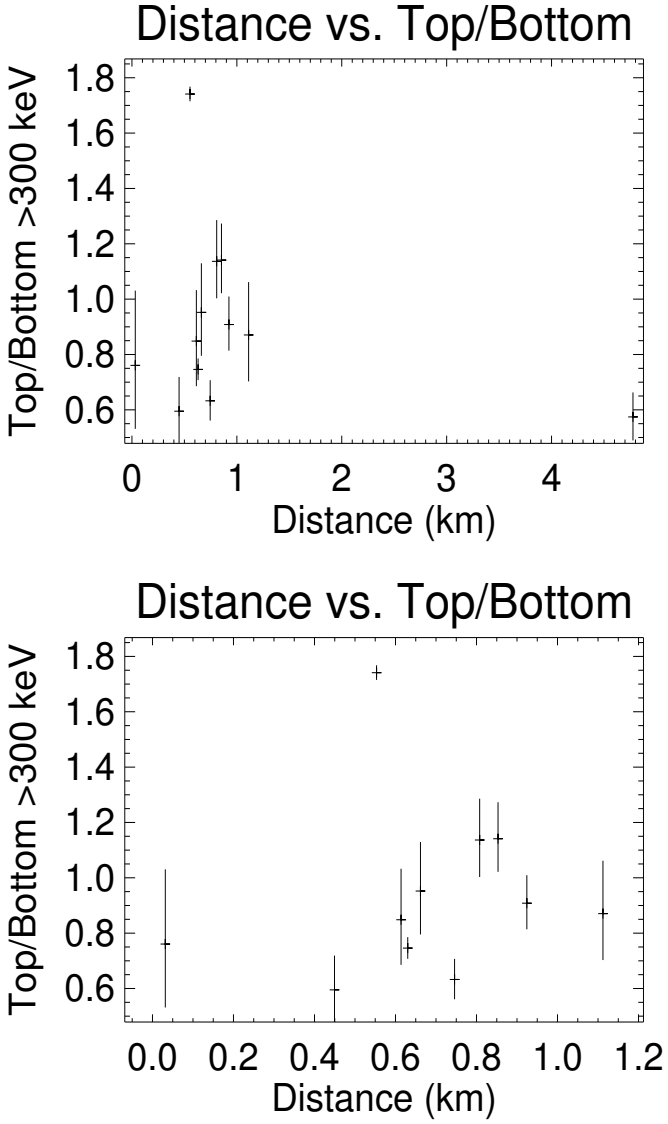


Figure 4.11: The glow top/bottom ratio >300 keV as a function of distance from an electrified cell.

This relationship is shown in Figure 4.13.

So far, we have used lightning near the ADELE instrument to determine liklihood of measuring a glow and to determine a distance to the glow. Lightning activity near the glow can give insight into the relationship between a glow and lightning, showing the overall electrification of the cloud. In top plot in Figure 4.14, the lightning activity before and after each glow is shown. The two populations are significantly different by 5.96 σ. The bottom plot in Figure 4.14 shows the lightning activity before and after the time when we would expect to measure a glow. These are when the lightning model predicts a glow but we do not measure one. These two populations are only different by 2.04 σ. There are no overlapping lightning flashes for these two plots.

There is more lightning activity before a glow than after it which could be explained two way: that glows are only able to form once the lightning activity has diminshed, so the electric field can reach the RREA threshold or that glows are discharging the cloud and suppressing lightning activity. Chapter 5 will show that a glow may be able to discharge as much as lightning for a short period of time, so the latter explanation may be correct.

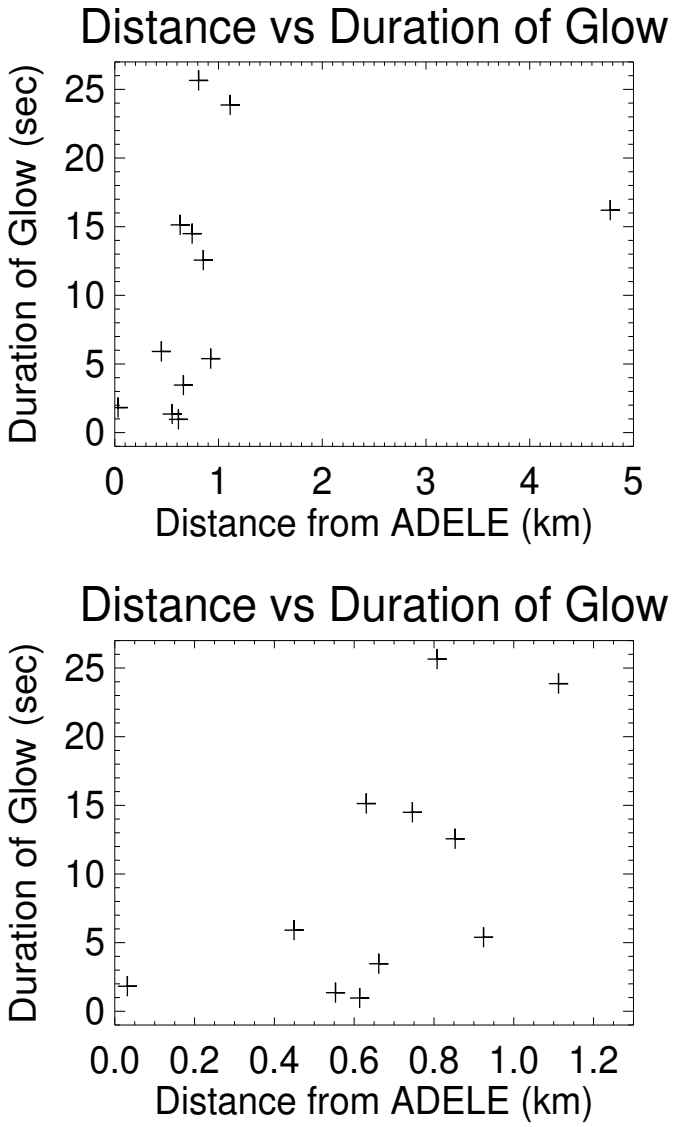


Figure 4.12: The duration of the glow as a function of distance to an electrified cell.

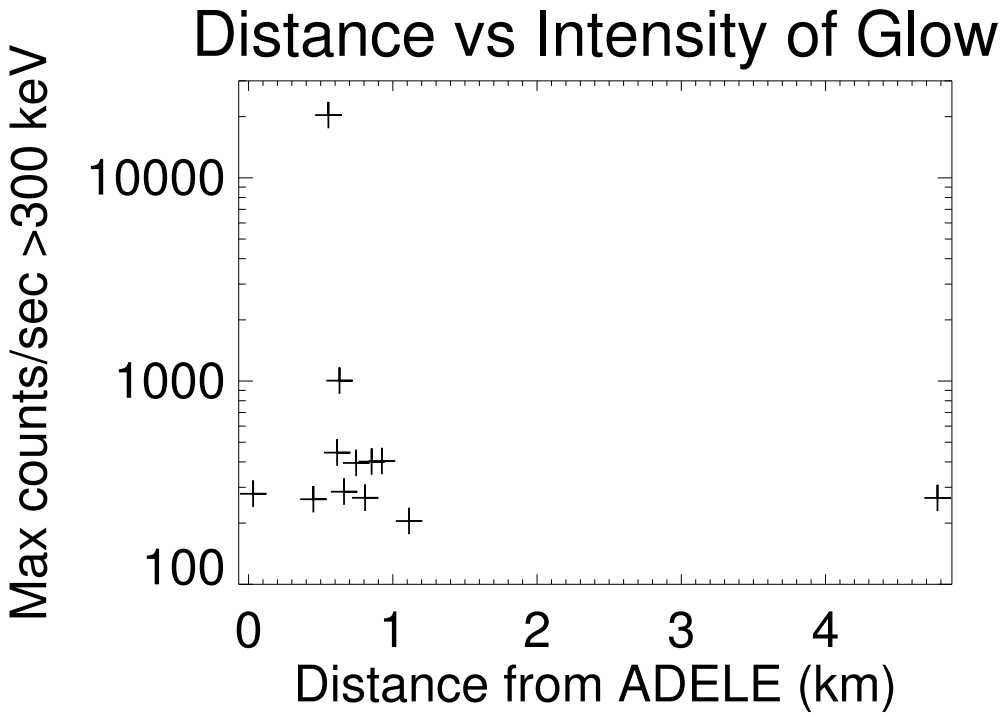


Figure 4.13: The peak intensity of the glow as a function of distance to an electrified cell.

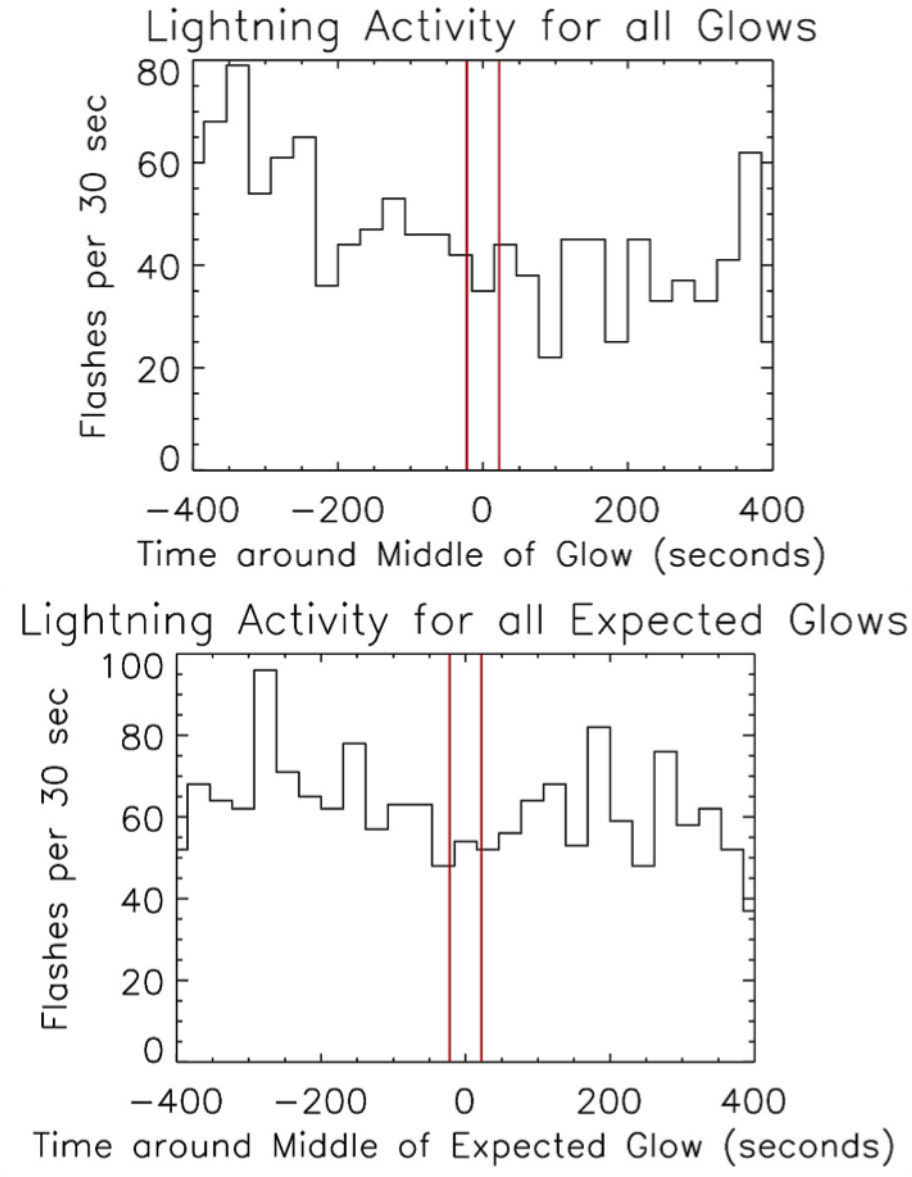


Figure 4.14: Top: Lightning flashes per 30 seconds within 20 km of each glow. The red lines show the average duration of a glow. Bottom: Lightning flashes per 30 seconds within 20 km of each expected glow. The red lines show the average duration of an expected glow.

Chapter 5

Relativistic electron avalanches as a thunderstorm discharge competing with lightning

5.1 Introduction

Gamma-ray glows lasting minutes or more have been observed to originate from thunderclouds (McCarthy & Parks, 1985; Eack et al., 1996a; Chubenko et al., 2000; Brunetti et al., 2000; Torii, Takeishi & Hosono, 2002; Tsuchiya et al., 2009; Chilingarian et al., 2010). Measurements of high-energy spectra suggest the presence of relativistic runaway electron avalanches (Tsuchiya et al., 2007; Babich

et al., 2010), the same process underlying terrestrial gamma-ray flashes (Dwyer & Smith, 2005). We demonstrate that glows with this spectrum are a very common phenomenon near the tops of thunderstorms. Examining the strongest glow measured by the Airborne Detector for Energetic Emissions (ADELE), we show that relativistic runaway electron avalanche (RREA) in the glow is occurring between the upper positive charge layer and the negative screening layer above it, and discharging the upper positive layer strongly enough to compete with lightning in discharging the storm. For this glow, the gamma-ray flux observed is close to the value at which relativistic feedback processes Dwyer (2012) become important.

The relativistic runaway electron avalanche (RREA) process was first proposed by Gurevich, Milikh & Roussel-Dupre (1992) to help explain the large flux of gamma rays seen by McCarthy and Parks in 1983 aboard a NASA F-106 airplane during a thunderstorm(McCarthy & Parks, 1985). Since then, several groups have measured glows from the ground (Chubenko et al., 2003; Brunetti et al., 2000; Torii, Takeishi & Hosono, 2002; Tsuchiya et al., 2009; Chilingarian et al., 2010) and from balloons (Eack et al., 1996a, 2000). It follows from C.T.R. Wilson's hypothesis in 1925 that energetic electrons in an electric field, such as those in thunderclouds, could accelerate to relativistic velocities even in fields where thermal electrons can not overcome atmospheric friction (Wilson, 1925). For the RREA mechanism, Gurevich, Milikh & Roussel-Dupre (1992) considered

the effect of Moller scattering. In this scenario, relativistic electrons elastically scatter with other electrons, thereby producing an avalanche of relativistic electrons. The electrons emit gamma rays as they slow down from interactions with air molecules. RREA is the generally accepted mechanism for explaining the incredibly bright and energetic Terrestrial Gamma-ray Flashes (TGFs) that have been seen by satellites. The spectrum of gamma-ray glows is similar to that of TGFs (Tsuchiya et al., 2007; Babich et al., 2010; Dwyer & Smith, 2005) but is orders of magnitude less bright.

In order to explain the brightness of TGFs, Dwyer proposed the relativistic feedback mechanism (Dwyer & Smith, 2005; Dwyer, 2012, 2008). We will show that during gamma-rays glows, the electric field is approaching the levels necessary for feedback but the field is not high enough to produce a TGF. The relativistic feedback process builds on the RREA process by including the physics of backscattered gamma rays and positrons from gamma-ray pair production, both of which propagate to the start of the avalanche region and generate new avalanches, producing an exponential growth in the number of avalanches.

As thunderclouds charge, RREA and therefore glows may produce a significant discharge current which can balance the charging of the cloud, with the bulk of the current coming from molecules ionized by the relativistic particle, not the energetic electrons directly (Dwyer, 2003; Dwyer, Smith & Cummer, 2012). Lightning is one

of the main mechanisms that can discharge thunderclouds (MacGorman & Rust, 1998). We demonstrate for the first time that glows can provide a comparably effective channel for thunderstorm discharge.

5.2 Results

The Airborne Detector for Energetic Lightning Emissions (ADELE) measured 12 gamma-ray glows during nine flights and 37 flight hours in the Colorado and Florida region. ADELE flew on a NCAR Gulfstream V during August and September of 2009. The glows were detected using two large 12.7 cm diameter, 12.7 cm long plastic scintillators. Each detector was in a separate aluminum box with the top detector having lead lining the bottom half of the plastic crystal and with the opposite configuration for the bottom detector. These detectors were read out by discriminators with energy thresholds of roughly 50 keV, 300 keV, 1 MeV, and 5 MeV.

We used a two stage Monte Carlo simulation to compare our results with the spectrum caused by RREA. The first stage propagates electrons generated by relativistic runaway through an exponential atmosphere at various altitudes. The Monte Carlo simulation includes all the relevant physics for describing energetic electrons and positrons along with the emission and propagation of energetic photons (Dwyer, 2003, 2007). The second stage takes the gamma rays, electrons,

and positrons that pass through the Gulfstream Vs cruising altitude of 14.5 km and feeds their energy, trajectory, and particle type through a GEANT3 (Brun, Carminati & Giani, 1993) model of the plane and ADELE to simulate the observed count rate in each discriminator channel.

ADELE observed 12 gamma-ray glows, three of which were double peaked due to multiple passes near the same glow region. A glow seen on 21 August is 20 times brighter than any other glow and therefore contains the best spectral information. Durations ranged from 4 to 112 seconds but these values, except for the 21 August glow, are most likely due to the planes motion rather than intrinsic variation, the spread being due to different sizes of the glow region and the varying lateral distance of the aircraft in each case. This is evident in the rise and falls times of the glows. These rise and fall times can be reproduced in models. The 21 August glow ends abruptly and much too quickly to be due to anything other than a rapid, lightning-like discharge of the cloud although no lightning was simultaneously detected. Figure 5.1 shows the 21 August glow compared to 3 other glows on different days, including all four energy channels. The significant counts in the >5 MeV channel rule out the spectrum of cold runaway emission from lightning leaders typically seen from the groundDwyer, Smith & Cummer (2012).

Taking the ratio of counts in the top and bottom detectors is not only use-

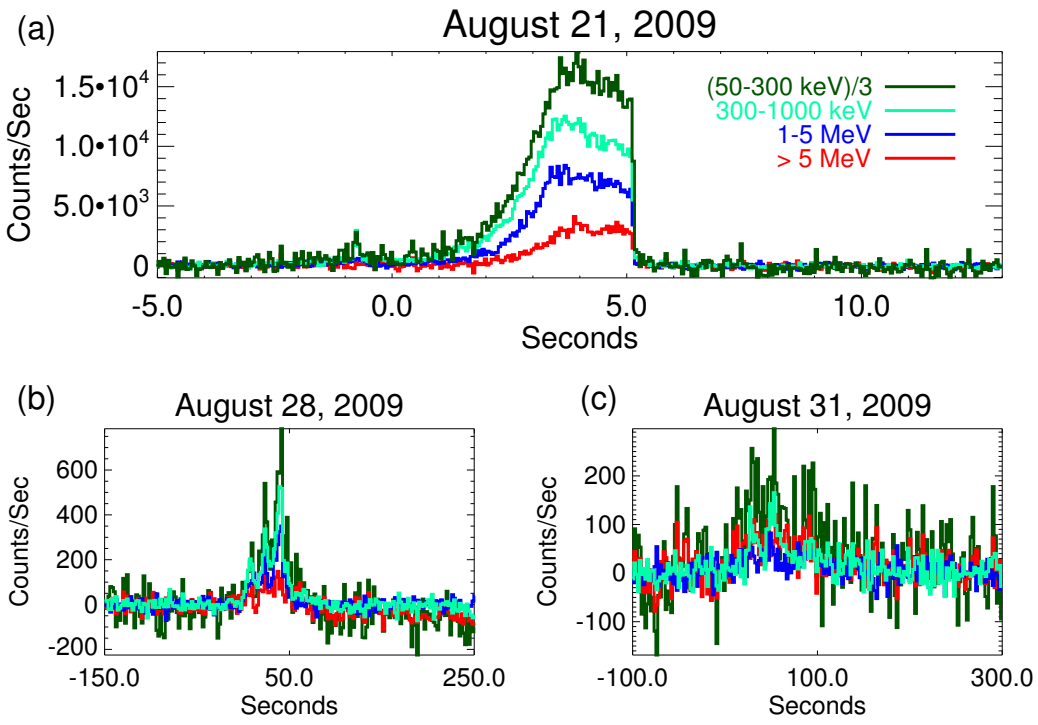


Figure 5.1: Time profile of three ADELE glows, summing both large plastic detectors. The lowest channel (dark green) is divided by three to show the higher energy channels more clearly. Background has been subtracted. (a) The brightest glow, on 21 August 2009 which had an abrupt ending; (b) and (c) two other more typical glows in which the instrument probably passed by but not through the avalanches.

ful for determining directionality, but is also sensitive to whether bremsstrahlung gamma-rays or the primary electrons themselves dominate the radiation field. The top/bottom ratio for 21 August increases for each channel. The ratios for the four channels at the peak of the glow are 1.76±0.02, 1.71±0.04, 1.98±0.06, and 5.79+0.59/−0.50. These high ratios can only be obtained in the simulations if ADELE is both directly in a downward avalanche and in the end of the avalanche where the vast majority of particles are electrons rather than gammas. The increase of top/bottom ratio for the top two channels is indicative of the large population of electrons being directed downward at the plane. The higher the energy of the electron, the more likely it will make it through the airplane exterior and interact with our detector.

The spectrum for the 21 August glow is also harder than it is for any other glow, and the simulations also show that this is consistent with being within the avalanche region, and not just the gamma-ray field above it. Figure 5.2 shows the charge geometry of the observed glow. For the altitude 14.1 km that the Gulfstream V was flying during the 21 August glow, ADELE must be between the main upper positive and negative screening layer. It is likely that the factor of 20 intensity difference between this glow and the others is that rest were observed only in the gamma-ray radiation field, above and laterally displaced from the avalanche itself; this is supported by the flight path data and lightning maps.

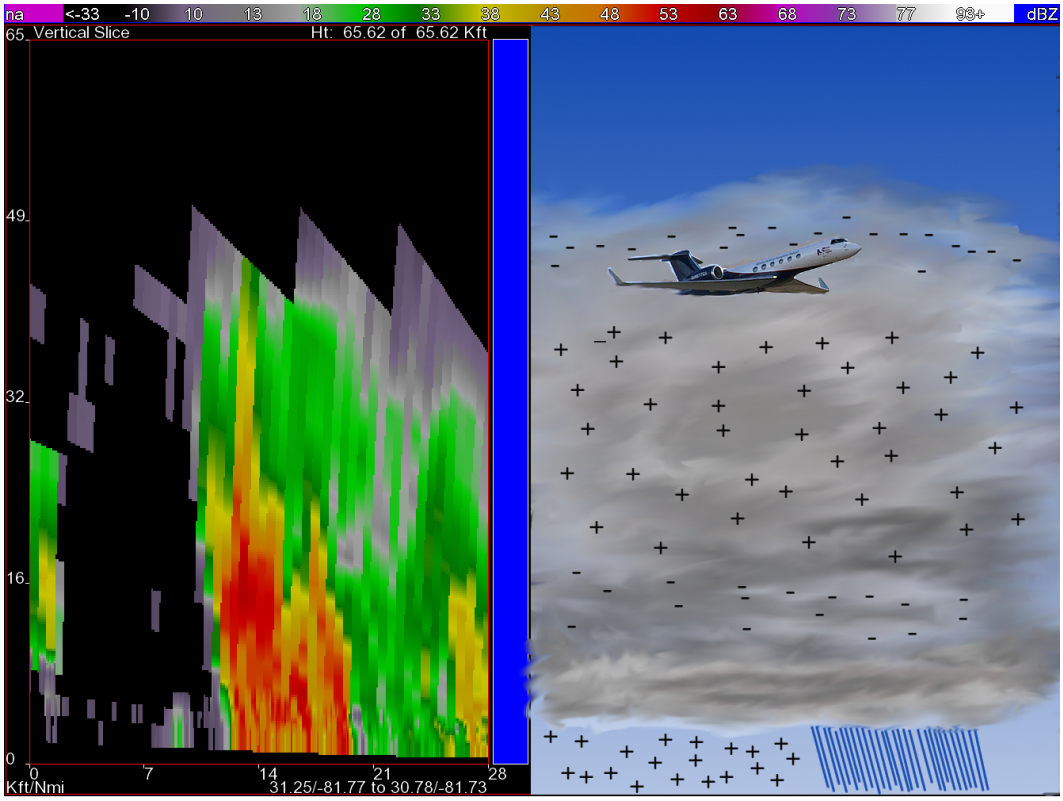


Figure 5.2: Left: the vertical cross section of reflectivity along the path of the plane during the 21 August glow. Right: a typical charge structure and the charges corresponding altitudes. The plane marks the altitude of ADELE during the glow.

From the peak brightness observed, we can conclude that the cloud was approaching the limit necessary for feedback for the electric field modeled, 400 kV/m, typical for a thunderstorm (Dwyer, 2003). Normalizing the results of our GEANT simulation, we find that the runaway electron fluence at the end of the avalanche is 1118.71 electrons/sec/cm^2. We assume a 1 MeV seed particle flux of 0.25 counts/sec/cm^2 from the cosmic ray background (Carlson, Lehtinen & Inan, 2008). This is an avalanche multiplication factor of 4475, close to but still less than 5000, where feedback begins to dominate.

Because gamma-ray glows persist for seconds, most of the discharge current resulting from runaway electrons will come from the drifting ions and not the low-energy electrons or runaway electrons (Dwyer, 2008). In the runaway electron avalanche region, the main source of ions is the ionization caused by the runaway electrons. Each runaway electron creates electron-ion pairs per unit length by ionizing the air. The low-energy electrons then attach to oxygen on the timescale of microseconds, forming negative ions. If we assume that the density of ions is not too large, ion-ion and ion-electron recombination may be ignored. The main loss of ions is then assumed to be attachment of ions to cloud ice and water particles. This attachment length, λ_{cl}, which depends on the density of cloud particles, the total water content, the charge on the cloud particles, and the electric field, is on the order of 1-10 m for typical thundercloud parameters (MacGorman & Rust,

1998; Dwyer, 2005; Chiu, 1978). For simplicity, we shall assume that this length is the same for positive and negative ions. The density of positive and negative ions, $n_{\pm}$, is then given by Equation 5.1.

$$\frac{dn_{\pm}}{dt} = \alpha F_{re} - \frac{n_{\pm}\mu_{\pm}E}{\lambda_{cl}} \tag{5.1}$$

F_{re} is the fluence (particles per m^2 per second) of runaway electrons; the ionization per unit length, $\alpha \sim 8350/\mathrm{m}\times N$, where N is the density of air relative to that at standard conditions (Dwyer & Babich, 2011); $\mu_{\pm}$ is the mobility of the ions; and E is the electric field strength. In the steady state, which should apply to glows, Equation 5.2 applies.

$$n_{\pm} = \frac{\alpha F_{re}\lambda_{cl}}{\mu_{\pm}E} \tag{5.2}$$

Using Equation 5.2, the electric current produced by the drifting positive and negative ions is given by Equation5.3.

$$J = en_{+}\mu_{+}E + en_{-}\mu_{-}E = 2e\alpha F_{re}\lambda_{cl} \tag{5.3}$$

For the observed runaway electron fluence of 1.12×10^7 electrons/m^2, this gives a discharge current density of 5-50 nA/m^2. This is comparable to the values between 1.4 and 2.3 nA/m^2 that we calculate from the rate of lightning in this storm cell using flash data from the United States Precision Lightning Network

(USPLN), and restricting ourselves to IC and +CG flashes, since they discharge the same layer. This range of mean lightning discharge is in agreement with a study (Livingston & Krider, 1978) done in 1978 for Florida lightning storms that found the lightning discharge rate to be 3 nA/m^2.

The frequency of glows that ADELE observed at cruise altitude despite not passing directly through as on 21 August demonstrates that the glow discharge process is not rare or anomalous. All of the other glows, except one, occurred when the Gulfstream V was passing near an active lightning cell. Glows were observed 11 out of the 149 times that we were close enough to an active electrified storm to observe them.

5.3 Conclusion

The brightest gamma-ray glow observed implies that RREA current played a significant role in that clouds discharging, competing with lightning. We also find that glows are a very common phenomenon between the upper positive and screening layer that may play an important role in the overall charge balance of thunderstorms, and perhaps electrified shower clouds, which by definition do not use lightning to discharge. All observed glows agree with the RREA spectrum; the glow on 21 August however, showed that sustained RREA can happen at a flux level requiring feedback. The glow spectrum from each of our large plastic

detectors on 21 August was consistent with a large population of energetic electrons above the plane and the gamma rays from bremsstrahlung below the plane. This geometry implies that ADELE is in the end of the avalanche region with the avalanche downward facing and therefore that the aircraft was flying between the main upper positive and negative screening layer.

5.4 Methods

The Airborne Detector for Energetic Lightning Emissions (ADELE) is an array of gamma-ray detectors that was originally designed to study TGFs from a plane. During its first campaign, it measured 12 gamma-ray glows and one TGF. We discuss the methods used for acquiring, processing and analyzing our glow data. The brightest glow on 21 August was analyzed most extensively and the uncertainties in modeling are addressed here.

In 2009, ADELE consisted of two sensor-heads, each with three scintillators, a plastic and NaI cylinder each 12.7 cm in diameter and 12.7 cm long and a plastic cylinder with a 2.54 cm diameter and 2.54 cm length all read out by photomultiplier tubes (PMTs). In the top sensor head, a 0.32 cm lead shield is placed along the bottom of each scintillator allowing those detectors to be more sensitive to radiation coming from above. The opposite is done in the bottom sensor head allowing the ratio of the top/bottom counts to give directionality. Signals from

the plastic scintillators PMTs are sent to discriminators at four energy thresholds, fast-chain electronic boards where the signal is split into four energy channels, approximately 50 keV, 300 keV, 1 MeV and 5 MeV. The discriminator outputs are sent to an FPGA where counts (rising edges) and deadtime are accumulated in 50 μs bins for every channel. The output from the NaI detectors was recorded only in a triggered mode that was not used in this work.

ADELE flew aboard a Gulfstream V operated by NCAR during August and September of 2009. The flights took place over regions near Colorado and Florida. During the 37 hours of flight that ADELE was onboard, 12 gamma-ray glows were seen, with some glows reappearing during multiple passes of the plane over the same cell.

After binning the counts of the large plastic detectors into two-second bins, the data were visually searched for glows. Glows were defined as series where the counts increased for more than two seconds. To ensure that we were not observing count rate changes due to altitude fluctuations of the airplane, a relationship between altitude and count rate was found during the ascent of the plane between 10 km and the cruising altitude (between 14 and 15 km). The effects from altitude were removed from all count rates.

To model the glow on 21 August, which was over 20 times brighter than any other glow in our data, we used a model of relativistic runaway avalanches with

positron and gamma-ray feedback (Dwyer, 2003, 2007). The output from this stage includes gamma rays, electrons, and positrons along with their energies and trajectories. These are then fed into a GEANT3 model (Brun, Carminati & Giani, 1993) that replicates the detectors, sensor heads, computers and electronics of the ADELE instrument and places them in a large aluminum cylinder that represents the Gulfstream V fuselage. Unfortunately, the exact mass distribution of the Gulfstream V is not known. This affects the top/bottom ratio and, less significantly, the energy spectrum that are given by our models. To account for this, we have modeled several extreme test cases to make sure our results are robust with the uncertainty. These include modeling an aluminum fuselage that is 40% of the total mass of the empty plane, no fuselage at all, and extra aluminum mass below the instrument. Figure 5.3 shows the best fit models from each of these test cases. The energy channels are known to within 10%. These best fit models feature top/bottom ratios that agreed in directionality, spectral models that are consistent with observations, and physically plausible geometries.

In order to calculate the lightning discharge rate that was occurring during the brightest glow on 21 August, lightning within 100 km and 10 minutes from ADELEs position when it measured the glow was used. The lightning was detected by the United States Preciscion Lightning Network (USPLN). Since the glow occurred between the upper positive and negative screening layer, the only types

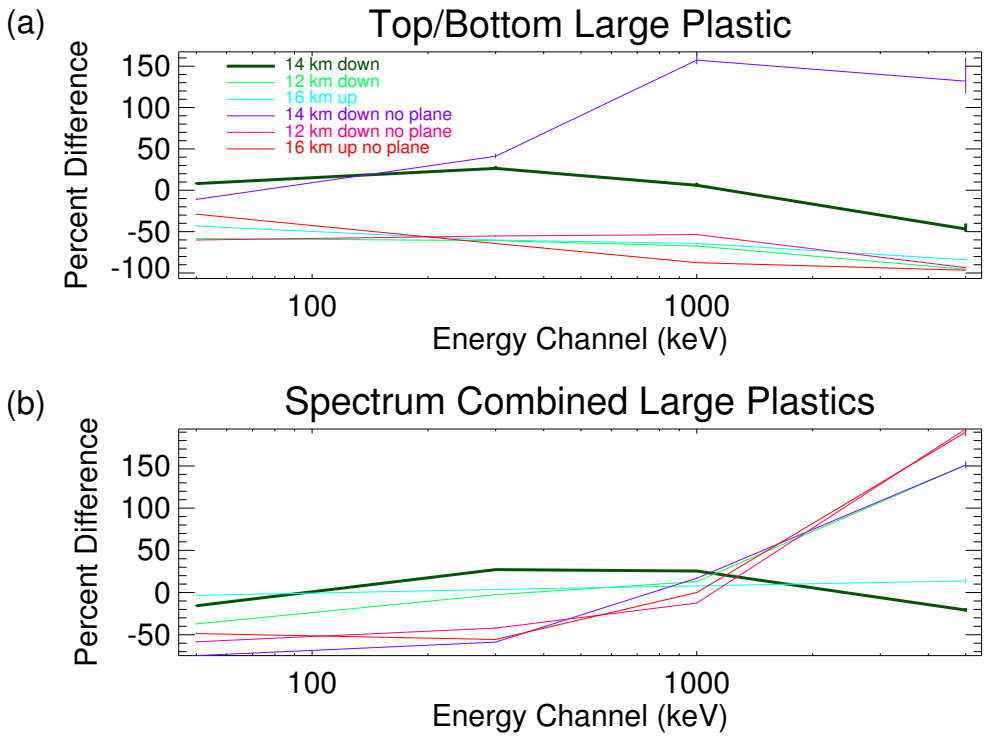


Figure 5.3: The percent difference between the ADELE data and various versions of the model that indicate different source altitudes and charge structures. (a) The percent differences between data and models for the top/bottom ratio of the two large plastic scintillators for each energy channel. (b) The percent differences for the summed (top plus bottom), normalized energy spectrum.

of lightning that could deplete that charge region are inner-cloud (IC) and positive cloud-to-ground (+CG) flashes. From Uman, Lightning Discharge it is assumed IC flashes carry 20 C mean charge (Uman, 2001) and from Lightning Physics and Effects it is assumed +CG flashes carry 80 C mean charge (Rakov & Uman, 2003). USPLN is much more sensitive to cloud-to-ground (CG) flashes than inner-cloud (IC) flashes so three methods were used to calculate the true amount of IC flashes. The first is from is that the ratio of IC/CG above Northern Florida is 2.5-3.0 (Boccippio et al., 2001). This yielded 1.4-1.7 nA/m^2. From Pierce, we can use $\frac{N_g}{N_c+N_g} = 0.1 + 0.25sin(\lambda)$ to determine the ratio of IC to CG flashes (Pierce, 1970). This yields a current density of 1.9 nA/m^2. The final method was from Prentice and Mackerras, the ratio of IC to CG is given by $\frac{N_c}{N_g} = 4.16 + 2.16cos(3\lambda)$ (Prentice & Mackerras, 1977). The discharge current from that ratio is 2.3 nA/m^2. These three methods are all in agreement with a previous calculation of the lightning discharge rate in a Florida storm that was 3 nA/m^2 (Livingston & Krider, 1978). All of these conclude that glows do compete with lightning as a method for discharging thunderstorms.

Chapter 6

Conclusion

In this dissertation, I have presented observations and analysis of gamma-ray glows seen by the ADELE instrument from a Gulfstream V airplane. I also discussed the version of ADELE that was used to measure glows and the newer version that is currently attempting to make measurements of glows and other high-energy atmospheric physics phenomena. All of the ADELE glows were presented, with details showing their relationship to lightning. One glow in particular, the glow on August 21, 2009, was reviewed most in-depth, as this glow was 20 times brighter than any other glow.

ADELE is the first instrument of its kind to be designed and optimized to study TGFs from an airplane. While the main science goal of the ADELE flights in 2009 was to measure TGFs, the instrumentation was also ideal to study glows.

Although only one TGF was detected, twelve gamma-ray glows were observed during the 2009 campaign, showing how relatively common glows are while highlighting how valuable portable instrumentation could be.

The ADELE instrument has gone through two major iterations. The first was designed to for the 2009 flights with scientists present to operate the instrument. It was a much larger layout because space was not an issue on these flights. The two data modes allowed for a continuous taking of data and a triggered mode of data acquisition. The second major iteration of ADELE made the instrument autonomous, more easily portable, and got rid of any triggered data acquisition. The newer version of ADELE makes the instrument easily adaptable to many flight situations. It was able to piggyback on two campaigns because of this adaptability: NASA's Hurricane and Severe Storm Sentinels and NOAA's Hurricane Hunters. This instrument may have flight opportunities in the coming years on NASA's ER2, as a piggyback again, and on the NSF's A10, as a primary science instrument.

The 12 gamma-ray glows detected by ADELE were all different. There seems to be intrinsic difference in the intensities of glows as the brightness is not a function of distance; although the distance is not precisely known. Except for the glow on August 21, 2009, which abruptly ends, glow duration appears to be a function of the amount of time that the instrument spends passing the glow. There is more lightning activity preceding a glow than following it, indicating a

relationship between glows and the overall charging of a cloud. This relationship to lightning can be understood as either the glows causing the suppression of lightning or that glows can only form once the lightning activity diminishes. In Chapter 5, I show that the glow on August 21, 2009 discharges the cloud as much as lightning so it suggests that glows may suppress lightning activity.

Since the glow on August 21, 2009 was 20 times brighter than any of the other glows thus allowing it to be analyzed most extensively, we learn more about glows, especially in the context of high-energy atmospheric physics and thunderstorm charging. I show that this glow is consistent with being directly in a downward facing avalanche, consistent with ADELE flying between the upper positive and negative screening layer at the top of a thunderstorm. The system approaches the levels necessary where feedback begins to dominate.

Work for the next version of ADELE has already begun. In addition, a new instrument, Gamma-ray Observations During Overhead Thunderstorms (GODOT), consisting of off-the-shelf data acquisition along with three detectors has been deployed in both Mexico and Japan. In Mexico, gamma-ray glows were observed on a mountain at 14,500 feet. At the time of writing, GODOT had just arrived to observe winter thunderstorms on the West coast of Japan. More glows like the glow on August 21, 2009 need to be observed in order to understand how common very bright glows are and their relationship to TGFs. When do bright glows hap-

pen versus a TGF? Also, how effective and common are these glows as a means to discharge thunderclouds? Glows could be a significant discharging mechanism and integral to understanding the overall charging of thunderstorms.

Bibliography

Babich L. P., Bochkov E. I., Donskoi E. N., Kutsyk I. M., 2010, Journal of Geophysical Research: Atmospheres (1984–2012), 115, A09317

Babich L. P., Bochkov E. I., Dwyer J. R., Kutsyk I. M., 2012, Journal of Geophysical Research: Atmospheres (1984–2012), 117

Boccippio D. J., Cummins K. L., Christian H. J., Goodman S. J., 2001, Monthly Weather Review, 129, 108

Briggs M. S. et al., 2010, Journal of Geophysical Research: Atmospheres (1984–2012), 115, A07323

Brun R., Carminati F., Giani S., 1993, GEANT detector description and simulation tool. CERN program library long writeup W

Brunetti M., Cecchini S., Galli M., Giovannini G., Pagliarin A., 2000, Geophysical Research Letters, 27, 1599

Carlson B. E., Lehtinen N. G., Inan U. S., 2008, Journal of Geophysical Research: Atmospheres (1984–2012), 113, A10307

Celestin S., Pasko V. P., 2011, Journal of Geophysical Research: Atmospheres (1984–2012), 116, A03315

Chilingarian A. et al., 2010, Physical Review D, 82, 043009

Chilingarian A., Hovsepyan G., Kozliner L., 2013, Physical Review D, 88, 073001

Chilingarian A., Mailyan B., Vanyan L., 2012, Atmospheric Research, 114-115, 1

Chilingarian A., Mkrtchyan H., 2012, Physical Review D, 86, 072003

Chilingarian A., Vanyan L., Mailyan B., 2013, Astroparticle Physics, 48, 1

Chiu C. S., 1978, Journal of Geophysical Research: Atmospheres (1984–2012), 83, 5025

Chubenko A. P. et al., 2003, Physics Letters A, 309, 90

Chubenko A. P. et al., 2000, Physics Letters A, 275, 90

Clay J., Jongen H. F., Aarts A. J. J., 1952, Physica, 18, 801

Cummins K. L., Murphy M. J., Bardo E. A., Hiscox W. L., Pyle R. B., Pifer A. E., 1998, Journal of Geophysical Research: Atmospheres (1984–2012), 103, 9035

Dwyer J. R., 2003, Geophysical Research Letters, 30, 2055

Dwyer J. R., 2004, Geophysical Research Letters, 31, L12102

Dwyer J. R., 2005, Geophysical Research Letters, 32, L20808

Dwyer J. R., 2007, Physics of Plasmas, 14, 042901

Dwyer J. R., 2008, Journal of Geophysical Research: Atmospheres (1984–2012), 113, D10103

Dwyer J. R., 2012, Journal of Geophysical Research: Atmospheres (1984–2012), 117, A02308

Dwyer J. R., Babich L. P., 2011, Journal of Geophysical Research: Atmospheres (1984–2012), 116, A09301

Dwyer J. R., Smith D. M., 2005, Geophysical Research Letters, 32, L22804

Dwyer J. R., Smith D. M., Cummer S. A., 2012, Space Science Reviews, 173, 133

Dwyer J. R., Smith D. M., Uman M. A., Saleh Z., Grefenstette B., Hazelton B., Rassoul H. K., 2010, Journal of Geophysical Research: Atmospheres (1984–2012), 115, D09206

Dwyer J. R., Uman M. A., 2014, Physics Reports, 534, 147

Eack K. B., Beasley W. H., Rust W. D., Marshall T. C., Stolzenburg M., 1996a, Journal of Geophysical Research: Atmospheres (1984–2012), 101, 29637

Eack K. B., Beasley W. H., Rust W. D., Marshall T. C., Stolzenburg M., 1996b, Geophysical Research Letters, 23, 2915

Eack K. B., Suszcynsky D. M., Beasley W. H., Roussel Dupre R., Symbalisty E., 2000, Geophysical Research Letters, 27, 185

Fishman G. J. et al., 1994, Science, 264, 1313

Gurevich A. V., 1961, Journal of Experimental Theoretical Physics, 12, 904

Gurevich A. V. et al., 2011a, Physics Letters A, 375, 4003

Gurevich A. V. et al., 2011b, Physics Letters A, 375, 1619

Gurevich A. V., Milikh G. M., Roussel-Dupre R., 1992, Physics Letters A, 165, 463

Halliday E. C., 1934, Mathematical Proceedings of the Cambridge Philosophical Society, 30, 206

Livingston J. M., Krider E. P., 1978, Journal of Geophysical Research: Atmospheres (1984–2012), 83, 385

MacGorman D. R., Rust W. D., 1998, The Electrical Nature of Storms. Oxford University Press, New York

Marisaldi M., Cattaneo P., 2010, J.Geophys.Res., 115, A00E13

Markwardt C. B., 2009, arXiv.org

Marshall T. C., McCarthy M. P., 1995, Journal of Geophysical ...

Marshall T. C., Rust W. D., Winn W. P., Gilbert K. E., 1989, Journal of Geophysical Research: Atmospheres (1984–2012), 94, 2171

McCarthy M., Parks G. K., 1985, Geophysical Research Letters, 12, 393

Moore C. B., Eack K. B., Aulich G. D., Rison W., 2001, Geophysical Research Letters, 28, 2141

Parks G. K., Mauk B. H., Spiger R., Chin J., 1981, Geophysical Research Letters, 8, 1176

Pierce E. T., 1970, Journal of Applied Meteorology, 9, 194

Prentice S. A., Mackerras D., 1977, Journal of Applied Meteorology, 16, 545

Rakov V. A., Uman M. A., 2003, Lightning: physics and effects

Saunders C., 2008, Planetary Atmospheric Electricity

Schonland B., 1930, ... of the Royal Society of London ...

Smith D. M. et al., 2011a, Journal of Geophysical Research: Atmospheres (1984–2012), 116

Smith D. M. et al., 2011b, Geophysical Research Letters, 38, n/a

Smith D. M., Hazelton B. J., Grefenstette B. W., Dwyer J. R., Holzworth R. H., Lay E. H., 2010, Journal of Geophysical Research: Atmospheres (1984–2012), 115

Smith D. M., Lopez L. I., Lin R. P., Barrington-Leigh C. P., 2005, Science, 307, 1085

Torii T., Sugita T., Kamogawa M., Watanabe Y., Kusunoki K., 2011, Geophysical Research Letters, 38

Torii T., Sugita T., Tanabe S., Kimura Y., Kamogawa M., Yajima K., Yasuda H., 2009, Geophysical Research Letters, 36, L13804

Torii T., Takeishi M., Hosono T., 2002, Journal of Geophysical Research: Atmospheres (1984–2012), 107, ACL 2

Tsuchiya H. et al., 2013, Physical Review Letters, 111, 015001

Tsuchiya H. et al., 2009, Physical Review Letters, 102, 255003

Tsuchiya H. et al., 2007, Physical Review Letters, 99, 165002

Tsuchiya H. et al., 2011, Journal of Geophysical Research: Atmospheres (1984–2012), 116, D09113

Uman M. A., 2001, The lightning discharge

Vonnegut B., Moore C. B., Semonin R. G., Bullock J. W., Staggs D. W., Bradley W. E., 1962, Journal of Geophysical Research: Atmospheres (1984–2012), 67, 3909

Whitmire D. P., 1979, Lettere Al Nuovo Cimento Series 2, 26, 497

Williams E. R., 1987, Scientific American, 259, 88

Wilson C. T. R., 1925, Mathematical Proceedings of the Cambridge Philosophical Society, 22, 534